NASA/TM—2000-209381/REV1

Directional Solidification of Pure Succinonitrile and a Succinonitrile-Acetone Alloy

James E. Simpson
Purdue University, West Lafayette, Indiana

Henry C. de Groh, III
Glenn Research Center, Cleveland, Ohio

Suresh V. Garimella
Purdue University, West Lafayette, Indiana

National Aeronautics and
Space Administration

Glenn Research Center

September 2000

Available from

NASA Center for Aerospace Information
7121 Standard Drive
Hanover, MD 21076
Price Code: A04

National Technical Information Service
5285 Port Royal Road
Springfield, VA 22100
Price Code: A04

Available electronically at http://gltrs.grc.nasa.gov/GLTRS

Directional Solidification of Pure Succinonitrile and a Succinonitrile-Acetone Alloy

James E. Simpson
School of Mechanical Engineering
Purdue University
West Lafayette, IN 47907-1288

Henry C. de Groh III
National Aeronautics and Space Administration
Glenn Research Center
Cleveland, OH 44135

Suresh V. Garimella
School of Mechanical Engineering
Purdue University
West Lafayette, IN 47907-1288

ABSTRACT

An experimental study of the horizontal Bridgman growth of pure succinonitrile (SCN) and of a succinonitrile–1.0 mol.% acetone alloy (SCN–1.0 mol.% ACE) has been performed. Experiments involving both a stationary thermal field (no–growth case) and a translating thermal field (growth case) were conducted. Growth rates of 2 and 40 μm/s were investigated. For the pure SCN experiments, the velocity field in the melt was estimated using video images of seed particles in the melt. Observations of the seed particles indicate that a primary longitudinal convective cell is formed. The maximum velocity of two different particles which traveled along similar paths was the same and equal to 1.49 ± 0.01 mm/s. The general accuracy of velocity measurements is estimated to be ±0.08 mm/s, though the data shows consistency to within ±0.02 mm/s. The shape of the solid/liquid interface was also quantitatively determined. The solid/liquid interface was stable (non–dendritic and non–cellular) but not flat; rather it was significantly distorted by the influence of convection in the melt and, for the growth case, by the moving temperature boundary conditions along the ampoule. It was found that the interface shape and position were highly dependent on the alignment of the ampoule in the apparatus. Consequently, the ampoule was carefully aligned for all experiments. The values for front location agree with those determined in previous experiments. For the alloy experiments, the solid/liquid interface was determined to be unstable at growth rates greater than 2.8 μm/s, but stable for the cases of no-growth and growth at 2 μm/s. When compared to the shape of the pure SCN interface, the alloy interface forms closer to the cold zone, indicating that the melting temperature decreased due to the alloying element. Extensive temperature measurements were performed on the outside of the ampoule containing pure SCN. The resulting thermal profiles are presented in detail in the results section. It is intended that the interface shape, thermal boundary condition and velocity data presented in this paper be used to test numerical simulations.

1. INTRODUCTION

Increasingly, advanced materials used in the aerospace, automotive, optical and electronic fields require low levels of defects and high levels of solute uniformity. Directional solidification by the Bridgman process is widely used for synthesis of these high–quality materials. During Bridgman crystal growth, heat and mass transfer by both (thermal and solutal gradient driven) convection and diffusion influence the shape of the solid/liquid interface and dopant segregation levels and hence directly determines the final crystal quality [1]. Key process parameters include the applied furnace temperature distribution and rate of translation, ampoule properties and furnace orientation.

Experimental investigations of solidification processes which involve metallic melts are complicated by the opacity, reactivity and high temperatures of the melts. Accurate experimental determination of the interface shape and convection is difficult. A means of reducing the difficulty, and increasing the accuracy, of solidification experiments is to use transparent materials that solidify in a manner analogous to metals. Experiments using such transparent metal analogs are widely reported in the literature [2–9]. Computer simulations are also employed to investigate solidification processes [10–15]. Such computer models are validated and enhanced by comparison with experimental results whenever these are available. Often the experimental data used for comparison purposes takes the form of thermal field and interface shape data [14, 15]. Obviously a much more complete and effective validation is achieved if experimentally determined velocity field data are available as well.

The aim of the current work is to perform detailed experiments of the Bridgman crystal growth process under terrestrial conditions. These results build on existing experiments performed under similar conditions [2]. Transparent metal analogs, namely pure succinonitrile (SCN) and a binary alloy of succinonitrile and 1.0 molar percent acetone (SCN–1.0 mol.% ACE), will be employed as the phase–change materials. Interface shape data will be obtained for both materials under no–growth and solidification conditions. Applied thermal field data will be obtained for the pure SCN sample under growth conditions. In addition, video images of seed particles moving in the melt

will be employed to estimate convective velocities in the pure SCN sample under no-growth conditions. It is hoped that the thermal boundary conditions, interface shape and melt convection velocity estimates will be used to validate numerical simulations of Bridgman growth. These simulations could then be used to optimize the Bridgman crystal growth process. An equipment list and a list of thermophysical properties of the SCN-ACE alloy used are provided in Appendix A.

2. EXPERIMENTAL SETUP

Test facility

The Transparent Directional Solidification Furnace (TDSF), located at the NASA Glenn Research Center, is shown schematically in figure 1 and pictured in figure 2. The TDSF furnace is a Bridgman type furnace with two copper jackets separated by an air gap which acts as the gradient or adiabatic zone between the two furnaces and also permits viewing of the glass ampoule which contains the phase change material. Constant–temperature circulating water baths provide the temperature set points for each jacket. The apparatus may be oriented in any direction; however, only the horizontal configuration is considered in this work.

The 150 mm long ampoules used are made of borosilicate glass with a square cross section. The ampoules are 8 mm on a side and have a wall thickness of approximately 1 mm. The thermal jackets have an 11 mm square hole running through their entire lengths into which the (smaller) ampoule is inserted. The thermal field imposed on the ampoule is complicated due to convection and conduction in the air surrounding the ampoule, and so, accurate alignment and centering of the ampoule within the jackets is essential to obtaining repeatable results. For growth experiments, a servomotor with reducing gear translates the cooling jackets at a desired constant velocity (2 or 40 μm/s for the present work). The motor and indexer are also able to position the jackets very accurately.

Ampoules containing pure SCN and an alloy of SCN doped with 1.0 mol.% (0.727 wt.%) ACE were used in this study. The ampoules were filled and sealed under vacuum conditions. For the ampoule

containing pure SCN, the material was first purified to eliminate any spurious solutal convection. The purification process involved distillation and zone-refining in a hermetically sealed glass unit [17]. Next, 63–90 μm diameter porous SiO_2 seed particles were added. These seed particles are used to resolve the velocities in the melt, the details of which will be explained below. For the alloy ampoule, the SCN was first purified and then a specific amount of acetone added (again under vacuum) to achieve the desired concentration level.

Interface locations

In previous work [2], interface shape measurements were obtained via the following procedure. Firstly, a 35 mm camera with a 10X zoom lens was used to photograph the interface in both the vertical and horizontal planes. These photographs were then developed offline. The interface locations were then measured from the prints using a digitizing tablet and pointer. The scale of the image was determined using the distance between the hot and cold furnace jackets on the image (which is known to be 5 mm on the apparatus). The primary sources of experimental error were uncertainties in the exact position of the interfaces, and uncertainties in determining the locations of the edges of the hot and cold furnaces, in the photographed image. For the present study, a somewhat modified technique was used. Interface positions were instead determined by analyzing images of the interface captured from the CCD video cameras. A sample interface image is shown in figure 4. The captured images were examined using image processing software. In some cases, rudimentary image filtering was employed to enhance the edges of the interface. Calibration was achieved in a similar manner as was used for the photographic analysis described above. The main advantages of using the CCD images rather than photographic prints are that results are obtained rapidly and that image processing software can be used to more easily detect interface positions. This technique is not believed to be any less accurate than using traditional photographic images. The experimental error in interface locations is estimated to be ±0.2 mm. Since the system is assumed to be symmetric in the x–z plane about the z axis, interfaces in x–z planes are averaged to produce symmetric results. Details of the averaging process are given in Appendix D. Both the raw and averaged data are provided in appendix C and D, respectively.

Temperature measurements

For measuring the thermal boundary conditions on the outside of the ampoule containing pure SCN, K-type (chromel-alumel) thermocouples were glued to the ampoule exterior. The instrumented ampoule used in previous work [2] was employed, which used a general purpose, low-conductivity epoxy to affix the thermocouples. The general arrangement of the thermocouples on the ampoule is shown in figure 5. A total of five thermocouples were used. These were placed mid-way between the bottom corners at (0, –4 mm, z), referred to as the Bottom Middle (BM) thermocouple, between the top corners at (0, 4 mm, z) called the Top Middle (TM) thermocouple, on the rear side wall (R) at (–4 mm, 0, z) and on the Bottom and Top Corners (BC and TC) at (–4 mm, –4 mm, z) and (4 mm, 4 mm, z), respectively. The thermocouple signals were recorded on a personal computer via a data acquisition system. Based on results from this and previous work [2] we advocate for the purpose of simplifying input boundary conditions for use in numerical simulations, that when all five thermocouple readings are being used, temperature be assumed to vary linearly around the periphery of the ampoule between the thermocouple locations. Care must be used if, for the purpose of simplifying input boundary conditions, any of the temperature data is omitted. For example, if it is desired to use only the top and bottom temperature measurements in the development of input boundary conditions, it may be better to impose an isotherm on the bottom wall and a linear profile around the rest of the ampoule periphery.

For the temperature measurements, data were obtained as follows. The starting position of the edge of the cold furnace was noted using the position encoder on the servomotor. The furnace was then translated until the edge of the cold furnace was in the same position as each thermocouple. In this way the locations of each thermocouple (relative to the start position) were found. Since measurements are taken under growth conditions, temperature readings were made at intervals of time corresponding to the furnace translating 1 mm (i.e. to take temperatures every 1 mm during the 40 μm/s growth case, temperatures were recorded every 25 seconds). A total of more than 40 measurements were obtained for each thermocouple for a given experiment.

The experimental error involved in locating the thermocouples is estimated to be ±0.3 mm. This error along with the finite thermal conductivity in the epoxies used to bond the thermocouples to the

outside of the glass ampoule and inherent thermocouple variability result in an estimated uncertainty of ±1 °C in the temperature readings.

Flow Visualization and Calculation of Melt Velocities

The motion of seed particles in the melt was filmed for a period of 10 minutes for the no-growth case. For the growth cases, particles near the interface were observed and filmed by sliding the cold furnace away from the interface zone to reveal the interface. This was done for time periods of a maximum of 40 seconds so as to minimize the impact of removing the cold furnace on the thermal condition on the outside of the ampoule and hence the results. The interface was observed to continue at the normal growth rate for this length of time; if the cold zone is removed for any longer the interface movement begins to slow down noticeably, indicating that the thermal conditions have been appreciably changed.

A novel lighting condition was employed to reveal the particles while minimizing glare from surfaces and defects. This involved pointing two focused beams from fiber-optic light sources equipped with polarizing filters along the axis of the ampoule, one directed from outside the hot zone towards the cold zone and one acting in the opposite sense. In this way, the transparent ampoule and phase change material behaved like a "light pipe". Lighting conditions are crucial to the acquisition of acceptable video images of the seed particle; no other positions for the light sources yielded acceptable results. The number density of particles in the melt was high, making flow visualization straightforward.

The following calibration procedure determines the magnification of the monitor image, enabling measurements of the flow velocities from the video. The coordinate system is drawn on the monitors midway between the copper jackets and along the longitudinal centerline of the ampoule (typical monitor images are shown in figure 3). It is estimated that the x, z and y, z origins were found to within ±0.13 mm. This error influences only the x, y, z locations of the particles tracked, not velocity determinations, which are subject to magnification and measuring errors. Magnification accuracy is estimated to be ±1.5%, and measuring uncertainty to be ±0.03 mm. The effect of measuring error is dependent on the velocity and can be very large at small velocities, since the distance traveled is small but the error (±0.03 mm) stays the same. Since velocities were measured

at approximately 0.5 sec. intervals, the measuring error can be translated directly to a velocity uncertainty of ±0.06 mm/s. It is also true that the particles will not move with the fluid exactly and will move at some velocity slower than the flow. An estimate of this difference can be obtained through comparison of the Stoke's settling rate, V_S, to a typical measured flow velocity of 1.46 mm/s, where $V_S = (2 \times 9.8\ m/s^2 \times (76 \times 10^{-6}\ m) \times 2 \times (1240\text{-}987)\ kg/m^3)/(9 \times 1.245\ kg/s\text{-}m) = 0.0025$ mm/s. Since V_S is very much less than the velocities we are attempting to measure, it can be said that the difference between the particle velocity and the actual flow velocity is negligible. Based on the uncertainties discussed above and data processing (which is discussed later) we judge the error in the velocity measurements to be no more than ±0.08 mm/s and the x and y locations of those velocities accurate to within ±0.16 mm and processed z locations accurate to within ±0.08 mm.

Particle locations in time, and thus flow velocities, were found using a three-step procedure. Firstly, the same suitable particle in both x–z and y–z views was found. Next, the particle location was marked with a dot on the monitors. The videotape was then advanced by a small amount (about 16 frames, or 0.5333 sec.) and the particle location was marked again. Finally, the distance from the dots to the axes was measured with a machinist's ruler and divided by the magnification. By commencing the second step when the particle enters the field of view and continuing until it leaves the field of view, a significant amount of (x, y, z, t) data for that particle can be obtained. A significant amount of judgment, expertise, and patience is required to find a single "good" particle in both views. For the purposes of this experiment, "good" particles are those with the following characteristics:

- Above average brightness
- Have a diameter no greater than slightly larger than average
- Not slower than nearby particles
- Travel near the vertical center plane (i.e. the 0, y, z plane)
- Be continuously visible throughout the entire time it is in the field of view
- Enter the field of view at the same time in both views
- Cross the (x, y, 0) plane at the same time in both views
- Have a zero z velocity component at the same time and at the same z coordinate on both x–z and y–z monitors

- No other particle present in either field that could be confused with the candidate particle

3. PURE MATERIAL (SCN) RESULTS

Temperature measurements

Thermal measurements for solidification at 2 μm/s and 40 μm/s were performed. The 40 μm/s growth case was considered mainly to provide a comparison between the current study and previous work [2], while the 2 μm/s results are needed to provide a comparison between the pure and alloy cases at this growth rate. The longitudinal thermal profile on the outside of the ampoule for the 40 μm/s growth case is shown in figure 6. For this experiment, the cold and hot zone temperature set points were 12 and 75 °C respectively, with an adiabatic zone length of 5 mm. Figure 6 is based on data averaged from two experiments; the values in these experiments agreed to within ±1 °C. The salient details about the temperature traces shown in figure 6 are as follows. The top middle (TM) and top corner (TC) thermocouples record the highest temperature values, while the bottom middle (BM) and bottom corner (BC) record the lowest values. This is in agreement with the observed interface shapes (refer to figure 8); solid is melted away from the top half of the domain indicating higher temperatures at the top of the ampoule. Once the melt is completely solid ($z < -7$ mm), convection in the ampoule ceases and the temperature traces trend to a single line. The values obtained in the current experiment agree reasonably well with those obtained in [2]. The majority of the results are within experimental uncertainty for all thermocouples; however some values for the top middle (TM) and rear middle (R) thermocouples in the −20 to −10 mm region differ by approximately 3 °C, which is larger than experimental uncertainty. A possible reason for this discrepancy could be a slight difference in the ampoule or furnace alignment than that used in [2]. The 2 μm/s growth case is shown in figure 7. For this experiment the temperature set points were 6 and 85 °C, with an adiabatic zone length of 1 mm. A de-humidifier was operated during the experiment to eliminate the formation of condensate droplets on the ampoule in the cold zone (which would affect the thermal boundary conditions in an uncontrolled manner). The key features of these temperature traces are similar to those reported for the 40 μm/s case (figure 6). The principal difference between these two cases is that the increased difference between the temperature set points, the decreased adiabatic zone length and slower growth rate has led to steeper temperature

gradients near the interface for the 2 μm/s case when compared to the 40 μm/s case. The temperature gradient at the interface temperature (58.08 °C) for the rear middle (R) thermocouple is 2.8 K/mm; this is increased from 1.2 K/mm for the 40 μm/s growth case shown in figure 6. No-growth results are particularly time consuming and were not attempted for the pure SCN case. Results for this case may be found in [2]. Tabulated data for the temperature profiles in figures 6 and 7 are in appendix B.

Interface locations

Interface shapes under no-growth conditions are shown in figure 8. Figure 8(a) details the front shapes in y–z (vertical) planes. The acronym MVP refers to the "mid vertical plane", which is the vertical plane running along the longitudinal centerline of the ampoule (0, y, z); FVP refers to the "front vertical plane", which is the vertical plane running along the inside of the front wall of the ampoule (3, y, z). The interface shape at the FVP should be identical to that at the rear vertical plane (–3, y, z) from symmetry. Note that the interface is considerably distorted from the vertical, with the solid forming a concave shape. The maximum deflection of the interface occurs along the MVP. The interface in this plane extends from a position of (0, –3, 2.09) to (0, 1.46, –2.00) – a total displacement of 4.09 mm. The FVP is not as severely deflected from the vertical as the MVP, ranging from (0, –3, 2.09) to (0, 2.92, –0.76). Figure 8(b) is a plot of the front shapes in x–z (horizontal) planes. The acronym MHP refers to the "mid horizontal plane", which is the horizontal plane through the height at which maximum interface deflection occurs (x, –1.6, z). BHP and THP refer to the horizontal planes running along the inside of the bottom and top ampoule walls respectively (x, –3, z) and (x, 3, z). The interface shapes in the MHP and THP are crescent-shaped, with the solid side being concave. There is slight asymmetry in the results, with the MHP interface meeting the front wall at (3, 1.5, –0.95) but the rear wall at (–3, 1.5, –0.99). This would tend to indicate that the ampoule was slightly misaligned such that the rear wall was closer to the furnace than the front wall. An interesting feature of figure 8(b) is the interface shape at the BHP. The interface meets the bottom wall at an acute angle and the contact line is difficult to quantify. Under ideal conditions this line should be symmetric since ideal thermal boundary conditions are both symmetric and steady. Observations during the course of this investigation have shown the shape of the interface at the BHP to be very sensitive to thermal conditions – the shape can often slowly

oscillate back and forth even if the remainder of the interface appears to be at steady state. As shown in figure 8(b), the interface in the BHP is not symmetric but is melted back closer to the rear wall, providing further evidence that the ampoule was slightly misaligned. Quantitative measurements of the interface shape at the BHP could not be determined in [2]. The distorted interface shapes indicate that convection in the melt region has a significant impact on thermal transport in the domain.

Interface locations for the 40 μm/s growth case are shown in figure 9. Figure 9(a) is a plot of the interface shapes in the MVP and FVP. As compared to the no-growth case, the interface has become much more elongated but has retained the same general shape. The location of the interface near the bottom wall is (0, –3.00, 0.17), while the point of maximum deflection is (0, 1.22, –6.92) – a total deflection of 7.09 mm, compared with 4.09 mm for the no-growth case. Considering the interfaces in the FVP and the MVP, the separation between the interfaces in the FVP and MVP is larger than for the no-growth case. Figure 9(b) is a plot of the interface shape in the horizontal mid plane (x, 1.5, z). Once again, this front is crescent shaped as in the no-growth case but is much more concave, with a smaller minimum radius of curvature. Interface locations in the other planes could not be determined quantitatively due to inadequate clarity of the CCD video images. The imposition of translating boundary conditions has led to the interface being much more distorted than for the no growth case (refer to figure 8(b)).

Interface locations for 2 μm/s growth conditions are shown in figure 10. Figure 10(a) is a plot of interface shapes in the MVP and FVP, while figure 10(b) is a plot of the interfaces in the BHP, MHP and THP. These interface shapes are similar to those found for the no-growth case. The key differences between the present case and the no-growth case are that the interfaces are slightly more compact (less total deflection in z) and that the interfaces are shifted back towards the cold zone; note that the furthest position of the MVP interface is (0, 1.46, –4.00) compared with (0, 1.46, –2.00) for no growth. Both these phenomena are a result of the *higher* thermal gradient imposed for this experiment. Had the thermal gradient imposed for the no-growth case been applied here we would anticipate that the total deflection of the interface would have increased slightly.

For Bridgman growth conditions, radial temperature gradients often exist in the adiabatic zone. Near the hot furnace, the sides of sample are warmer than the center; heat is transferred to the sample. The converse applies in the adiabatic zone near the cold furnace. These radial temperature gradients due to the applied thermal condition may influence the interface shape. Under growth conditions additional radial thermal gradients are produced since the temperatures in the sample lag behind those of the (translating) furnace due to the finite thermal conductivity of the sample. For the Bridgman growth of metals under conduction–dominated conditions, these radial gradients result in an interface shape that is slightly concave or convex [10]. For the cases shown in this work, horizontal Bridgman growth is considered. Observations made for SCN using the same apparatus as in this work but in the *vertical* Bridgman configuration (minimizing convection) reveal that the interface is flat during no–growth [20]. Thus the concavity and asymmetry of the interface shapes shown in figure 8 during no-growth is due to natural convection. The interface concavity and asymmetry in the growth cases, figures 9 and 10, are caused by both convection and conduction effects.

A comparison between the results shown in the present study and those in [2] for the no-growth and 40 μm/s cases yields the following comments. The majority of interface locations agree to within experimental error. For the more distinct and clearly defined interfaces (such as those in the MVP for the no growth case) agreement was particularly good – often to within 0.05 mm. For some of the less distinct interfaces, agreement deteriorated. The maximum difference was observed to occur for some points near the ampoule walls for THP and MHP interfaces, with discrepancies of approximately 0.4 mm, which is nearly greater than experimental error. The most serious discrepancy occurred for the 40 μm/s case in the MVP. Figure 11 is a plot of the two sets of results. Over the range (0, –3, z) to (0, 1.5, z) the results are in good agreement; however the results diverge for larger y values. This discrepancy warrants further discussion. Near the walls of the ampoule, there are often multiple reflections and determining the exact location of the interface can be difficult. Photographic and CCD images of the interface for the 40 μm/s growth case indicate a number of interface-like lines in the region marked "A" on figure 11. Exactly which line corresponds to the "true" mid plane interface is not immediately obvious merely by examining the interface images. The solution to this dilemma is to review the video images of seed particles

recorded for this case. Perusal of the videotape reveals that several particles entrained in the liquid cross the interface "B" and travel through the region marked "A"; but none cross interface "C", Therefore, it is concluded that the interface given by line "C" is the valid interface for this region.

Tabulated interface shape data for the cases described in figures 8, 9 and 10 may be found in appendices C and D.

Melt velocities

The following general observations about the flow patterns in both the no-growth and growth cases can be made. Footage of the ampoule from the side (i.e. images of the y–z plane) reveal a single, longitudinal, primary convective cell. The flow moves along the top wall towards the interface; as it approaches the (cold) interface it is forced down and away from the interface in an arc shaped in a "reverse–C". The paths that particles travel near the interface resemble the shape of the interface itself. The fluid returns to the hot melt region by traveling along the bottom wall away from the interface. This general description of the flow is true for both the no-growth and growth cases. Particles that travel near the interface are clearly affected by the viscous layer near the wall and are noticeably slower. Some particles were observed to travel very near the interface and drift very slowly. Occasionally, these particles would become entrained in the approaching front for the growth case. Observations of the ampoule from above (i.e. images of the x–z plane) reveal the secondary flows present near the interface. Particles which travel toward the interface along the centerline of the ampoule are forced downward as they approach the interface and return towards the hot zone along the centerline (i.e. zero movement in the x direction). A particle which is adjacent to the centerline will be forced outward from the centerline as it nears the interface. Such a particle then slides down the interface (thus the flow is clearly influenced by the shape of the interface) and returns to the bulk. These observations indicate that the convective flow is primarily a single two-dimensional cell in the y–z plane with secondary convective motions in x directions near the interface. Similar flow structures have been reported elsewhere [18].

In an effort to improve the data, the raw (x, z_x, t_x) and (y, z_y, t_y) data were processed in a manner similar to that discussed on page 5 of [2]. The data were processed based on two assumptions.

Firstly, it was assumed that the z values of the particle in the x–z and y–z views should be the same for the same time values and the minimum z value should be the same in the two data sets (x, z_x, t_x and y, z_y, t_y for a given particle). The seconds assumption was that the video for the two views might not be exactly synchronized – one set of data (x, z_x, t_x for example) might be slightly shifted in time relative to the other data set (y, z_y, t_y) for a given particle.

In correcting the data based on the first assumption, a set of data was created that consisted of a column of all the times from both x–z and y–z data sets. Then interpolated z_x values from the x, z_x data set were found at the measured times from the y, z_y data set, t_y. Then z_y values from the y, z_y data were interpolated to find z_y values at the t_x times from the x, z_x data. Now for every t_x we have a measured z_x value and an estimated z_y value, and for every t_y value we have a measured z_y value and an estimated z_x. For a given time, the z_x and z_y values should be equal. Also, it is simple to find the minimum z values in each x, z_x, t_x and y, z_y, t_y data set for a particular particle; these minima should also be equal (the minima should also occur at the same time, but may not due to the cameras being slightly out of sync). The differences between z_x and z_y values may be due to measuring errors or error in the placement of the axes, or video synchronicity error; recall the estimated error associated with the location of the origins of the axes is about four times the error expected from measuring, and that the x, z_x and y, z_y data are being obtained from different monitors. The z minima are independent of time and are a direct estimate of the error caused by inaccuracies in the placement of the axes; this is the starting point for correction of the data. For particle #13, the minimum z_x value is -1.807 mm, the minimum z_y value is -1.61 mm. Thus in an effort to minimize errors and inconsistencies in the data, we start by adding half the difference to the z_x values and subtracting half the difference from the z_y values. The average deviation between the z_x and z_y values at common time is monitored and minimized by varying this set value added to z_x and subtracted from z_y. In this way the systematic error most likely caused by errors in the placement of the axes can be minimized. A error minimum was found (for particle #13) by adding 0.08 mm to the z_x values and subtracting 0.08 mm from the z_y values. The average z deviation at a given time for the raw data (particle #13) was 0.165 mm, and after correcting by adding and subtracting 0.08 mm the average deviation was 0.040 mm.

After minimizing the differences in z (based on the first assumption), it was noted that the z_x values were consistently larger than the z_y values for incoming flow (−z velocity) and consistently smaller for returning (+z velocity) flow. This trend would be characteristic if a time lag was present in one of the data sets. Thus based on the second assumption, a shift in time was imposed on the y, z_y, t_y data. This time shift was varied (in increments of 0.0333 seconds = 1 video frame) and the average difference between the z_x and z_y values again minimized. The lowest deviation in z for particle #13 resulted with a time shift of 0.03333 seconds (added to t_y), which is equal to the video monitors being out of sync by one frame (one out of 30 frames/sec).

The amounts added to z_x and subtracted from z_y for particles #8, #12 and #13 were 0.1, 0.043, and 0.08 mm respectively. The time shifts imposed on the y, z_y, t_y data for particles #8, #12 and #13 were −0.03333, +0.03333, and +0.03333 seconds respectively. The average difference among the z_x and z_y values at each time before processing were 0.199, 0.0862 and 0.165 mm for particles #8, #12 and #13, respectively. After processing these differences had decreased to 0.0655, 0.0286 and 0.0218 mm, respectively. These results imply that after data processing, z values are being determined to within about ±0.04 mm (which is about equal to the measuring error originally estimated, thus errors due to placement of the axes and synchronicity have been nearly eliminated).

Tables F.1, 2, and 3 in Appendix F provide the raw, unprocessed (x, z_x, t_x) and (y, z_y, t_y) data from the video for particles denoted as #8, #12, and #13 respectively, for the no-growth, pure SCN case. Tables F.4, 5, and 6 provide the processed data for the particles tracked. Velocity measurements from three particles obtained for the no-growth case are shown in figure 12 and tabulated in Tables F.7, 8 and 9. The motion of the fluid particles shown in figure 12 corresponds well with the qualitative description provided above and with previous numerical simulations [8, 14-16].

4. ALLOY (SCN-ACE) RESULTS

Figure 13(a) is a plot of interface shapes in the MVP and FVP (abbreviations are explained in section 3) for the no-growth alloy case. The interface shape in the MVP bears a striking resemblance to that for the pure SCN case (see figure 8(a)). The key difference is the location of the interface. The

lowest z location for the alloy interface is –3.68 mm, whereas the lowest z location for the pure SCN case is –2.04 mm. The change in position is clearly due to the suppression of the interface temperature by the addition of the alloying substance. Figure 13(b) is the corresponding plot of the interface in the MHP. The curvature of the front in this plot is not as large as for the pure SCN case which agrees with the observed position of the FVP in figure 13(b).

Figure 14(a) is a plot of the interface in the MVP and FVP for the alloy 2 μm/s growth case. As in the no-growth case, the MVP alloy interface shape has a shape which is very similar to the pure material 2 μm/s growth case (figure 10(a)), while the values for the FVP interface are pushed slightly closer to the MVP results. The maximum deflection ($z_{max} - z_{min}$) for the alloy and pure 2 μm/s growth cases are about the same, 4.15 mm and 4.00 mm respectively. Tabulated data for the interface shapes in figures 13 and 14 may be found in appendices C and D. Upon examination of the ampoule temperature measuements for alloy 2 μm/s growth case, it was found that the temperature values were not reliable and thus they are not included in this paper. Failure of the alloy ampoule prevented further experimentation.

5. CONCLUSIONS

The horizontal Bridgman crystal growth of pure succinonitrile (SCN) and a succinonitrile–1.0 mol.% acetone (SCN–ACE) alloy has been experimentally investigated. Temperature profiles and interface shape data obtained for pure SCN agrees reasonably well with data found in a previous study [2]. The interface shapes for pure SCN are stable and non-dendritic; however they are not flat but instead assume a complex three-dimensional shape. This indicates the presence of thermally driven convective motion in the melt region which influences the interface shape.

Flow visualization for the pure SCN sample indicates that a single longitudinal convective cell forms, with warm fluid approaching the interface from the top of the domain, falling at the cool interface and retreating along the bottom of the ampoule. This cell is primarily two-dimensional – the only secondary flows observed occur near the interface and act to push approaching fluid out from the centerline toward the side walls. Convective velocities for the pure SCN sample under no-

growth conditions were measured using seed particles tracked by two orthogonal video cameras. The maximum velocity of two different particles which traveled along similar paths was the same and equal to 1.49 ± 0.01 mm/s. The general accuracy on velocity measurements is estimated to be $\pm$ 0.08 mm/s, though the data shows consistency to within $\pm$ 0.02 mm/s.

Interface shapes for the alloy appear to be similar in nature to those determined for the same conditions using pure SCN and so are influenced by thermally driven convection. The interfaces occur at lower temperatures than for the pure SCN case. This is a result of the suppression of the interface temperature due to the introduction of the solute. Growth of the alloy was experimentally found to be unstable and dendritic for growth velocities above 2.8 μm/s, at a temperature gradient of approximately 2.4 K/mm. Temperature measurements similar to those for the pure SCN case but for the alloy sample were attempted, however examination of the alloy temperature measurements revealed that they were erroneous and so were not included in the present study. Further experiments to obtain temperature and velocity measurements for the alloy sample are planned as future work.

REFERENCES

[1] M. C. Flemings, *Solidification Processing*, McGraw-Hill, 1974.

[2] H. C. de Groh III and T. Lindstrom, "Interface Shape and Convection During Solidification and Melting of Succinonitrile," *NASA Technical Memorandum 106487*, June 1994.

[3] S. V. Garimella, J. P. McNulty and L. Z. Schlitz, "Formation and Suppression of Channels during Upward Solidification of a Binary Mixture," *Metall. and Mater. Trans. A*, Vol. 26A, pp. 971-981, 1995.

[4] C. S. Magirl and F. P. Incropera, "Flow and Morphological Conditions Associated with Unidirectional Solidification of Aqueous Ammonium Chloride," *Topics in Heat Transfer, ASME HTD-Vol. 206*, pp. 1-9, 1992.

[5] A. Hellawell, J. R. Sarazin and R. S. Steube, "Channel convection in partly solidified systems," *Phil. Trans. R. Soc. Lond. A*, Vol. 345, pp. 507-544, 1993.

[6] S. M. Copely, A. F. Giamei, S. M. Johnson and M. F. Hornbecker, "The Origin of Freckles in Unidirectionally Solidified Castings," *Met. Trans.*, Vol. 1, pp. 2193-2204, 1970.

[7] S. de Cheveigné, C. Guthmann and M.-M. Lebrun, "Nature of the Transition of the Solidification Front of a Binary Mixture from a Planar to a Cellular Morphology," *J. Crystal Growth*, Vol. 73, pp. 242-244, 1985.

[8] M. A. Eshelman, V. Seetharaman and R. Trivedi, "Cellular Spacings—I. Steady-State Growth," *Acta Metallica*, Vol. 36, No. 4, pp. 1165-1174, 1988.

[9] M. A. Eshelman, V. Seetharaman and R. Trivedi, "Cellular Spacings—II. Dynamical Studies," *Acta Metallica*, Vol. 36, No. 4, pp. 1175-1185, 1988.

[10] P. M. Adornato and R. A. Brown, "Convection and Segregation in Directional Solidification of Dilute and Non-Dilute Binary Alloys: Effects of Ampoule and Furnace Design," *J. Crystal Growth*, Vol. 80, pp. 155-190, 1987.

[11] M. C. Liang and C. W. Lan, "Three-Dimensional Convection and Solute Segregation in Vertical Bridgman Crystal Growth", *J. Crystal Growth*, Vol. 167, pp. 320-332, 1996.

[12] J. E. Simpson and S. V. Garimella, "An investigation of the solutal, thermal and flow fields in unidirectional alloy solidification", *Int. J. Heat Mass Transfer*, Vol. 41, No. 16, pp. 2485-2502, 1998.

[13] X. Zeng and A. Faghri, "Temperature-Transforming Model for Binary Solid-Liquid Phase-Change Problems Part II: Numerical Simulation," *Numer. Heat Transfer*, Part B, Vol. 25, pp. 481-500, 1994.

[14] M. Yao and H. C. de Groh III, "Three-Dimensional Finite Element Method Simulation of Bridgman Crystal Growth and Comparison with Experiments," *Numer. Heat Transfer*, Part A, Vol. 24, pp. 393-412, 1993.

[15] G. H. Yeoh, G. de Vahl Davis, E. Leonardi, H. C. de Groh III and M. Yao, "A Numerical and Experimental Study of Natural Convection and Interface Shape in Crystal Growth," *J. Crystal Growth,* Vol. 173, pp. 492-502, 1997.

[16] H. C. de Groh III and M. Yao, "Numerical and Experimental Study of Transport Phenomena in Directional Solidification of Succinonitrile," *Transport Phenomena in Solidification, ASME HTD-Vol. 284,* pp. 227-243, 1994.

[17] M. A. Chopra, M. E. Glicksman, and N. B. Singh, *Metallurgical Transactions A*, Vol. 19A, 1988, p. 3087.

[18] G. J. Merchant and S. H. Davis, "Shallow Cells in Directional Solidification," *Physical Review Letters,* Vol. 63, No. 5, pp. 573-575, 1989.

[19] B. B. Miller, M. B. Meyer and M. D. Bethea, "Stereo Imaging Velocimetry for Microgravity Applications," *Procs. International Symposium on Space Optics, SPIE-Vol. 2210,* pp. 260-270, 1994.

[20] C. Mennetrier, M. A. Chopra and H. C. de Groh III, "Effect of Thermal Convection on the Shape of a Solid-Liquid Interface," *Forum on Microgravity Flows, ASME FED-Vol. 111,* p. 5, 1991.

[21] Chopra, M.A., *Ph.D. Thesis,* Rensselaer Polytechnic Institute, 1984.

[22] Glicksman, M.E., Scheafer, R.J. and Ayers, J.D. *Metall. Trans. A*, 1976, Vol. 7A, pp. 1747-1759.

[23] Y.S. Touloukian, R.W. Powell, C.Y. Ho and P.G. Klemens, *Thermophysical Properties of Matter,* IFI/Plenum, Vol. 2, pp.922-932, 1970.

[24] D.L. Ceynar and C. Beckermann, "Measurement of the Density of Succinonitrile-Acetone Alloys," *University of Iowa,* (unpublished research), 2000.

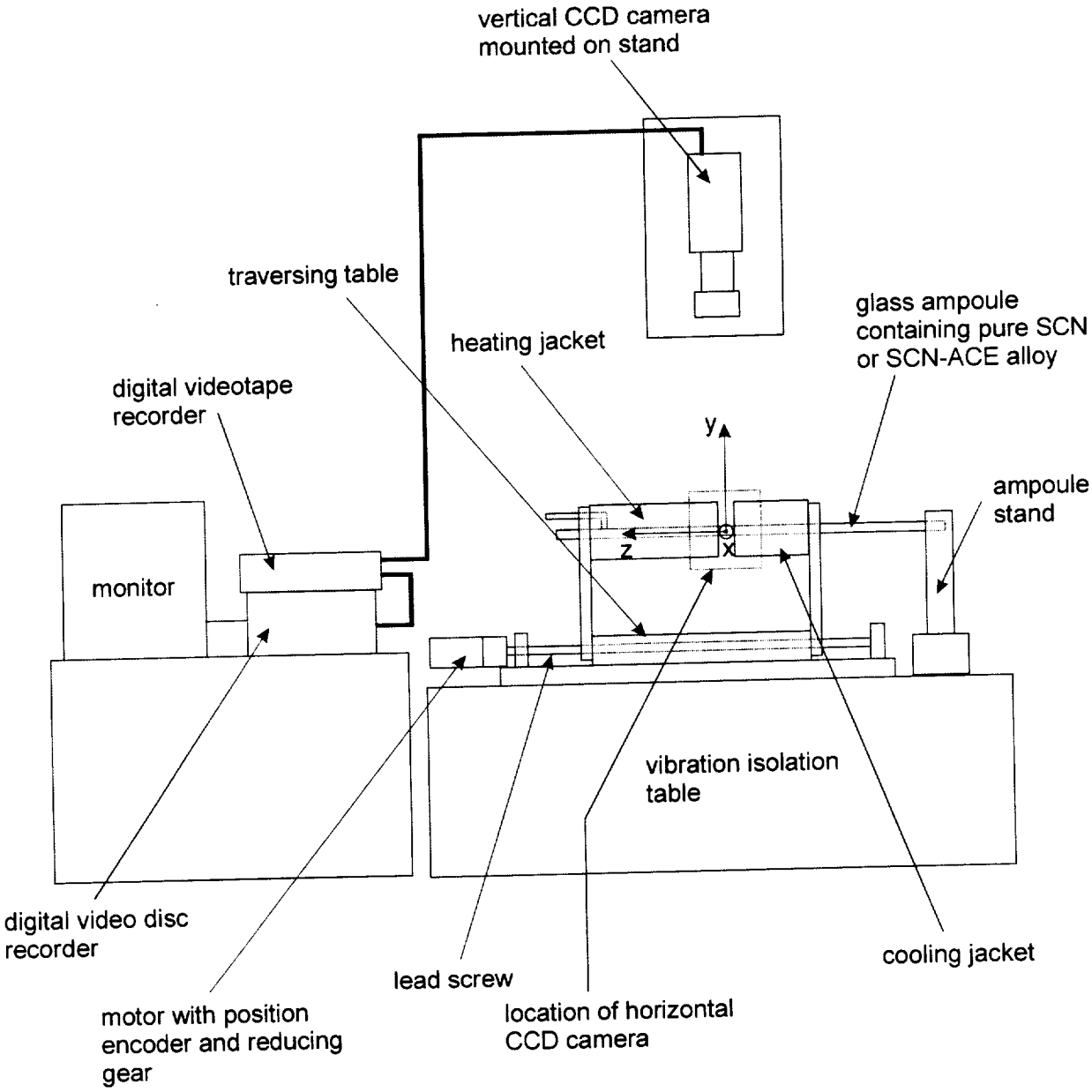

Figure 1. Schematic of NASA's Transparent Directional Solidification Furnace (TDSF). Note that an additional CCD camera setup (including camera, digital video tape recorder, digital video disc recorder and monitor like the one pictured) is not shown for clarity. This camera points directly down into the page. The position of the camera is indicated by the broken outline.

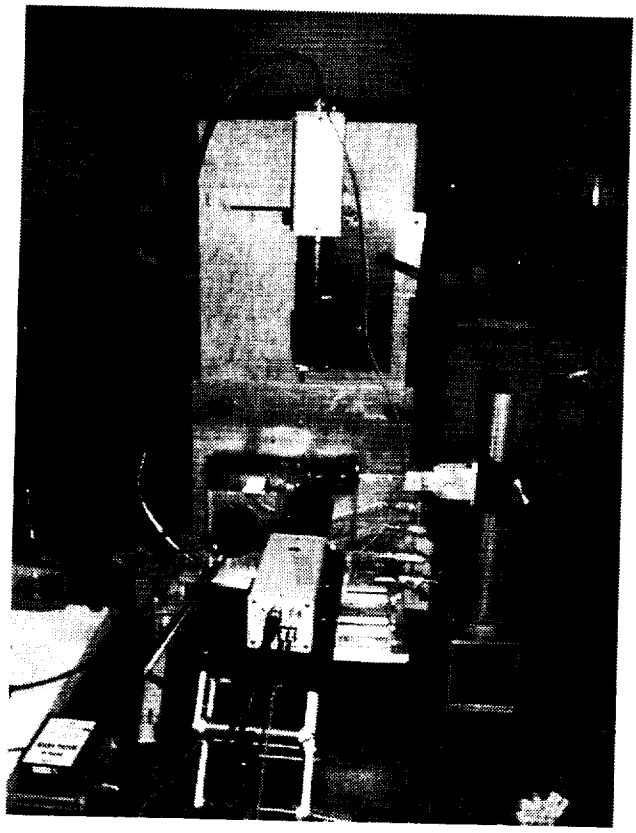

(a)

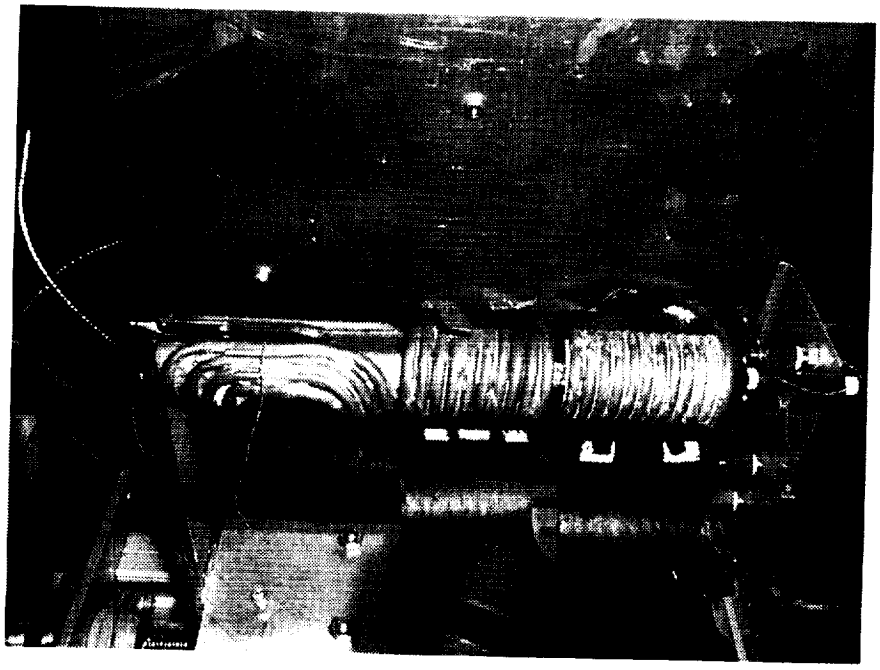

(b)

Figure 2. Photographs of (a) overview of the experimental setup, including the CCD cameras in the vertical and horizontal planes and (b) close-up of the copper heating and cooling jackets (with insulation removed to reveal the tubing). Note the gap between the heating and cooling jackets; this serves as the gradient zone. Both the hot and cold jackets can temporarily slide left or right to permit viewing of the interface.

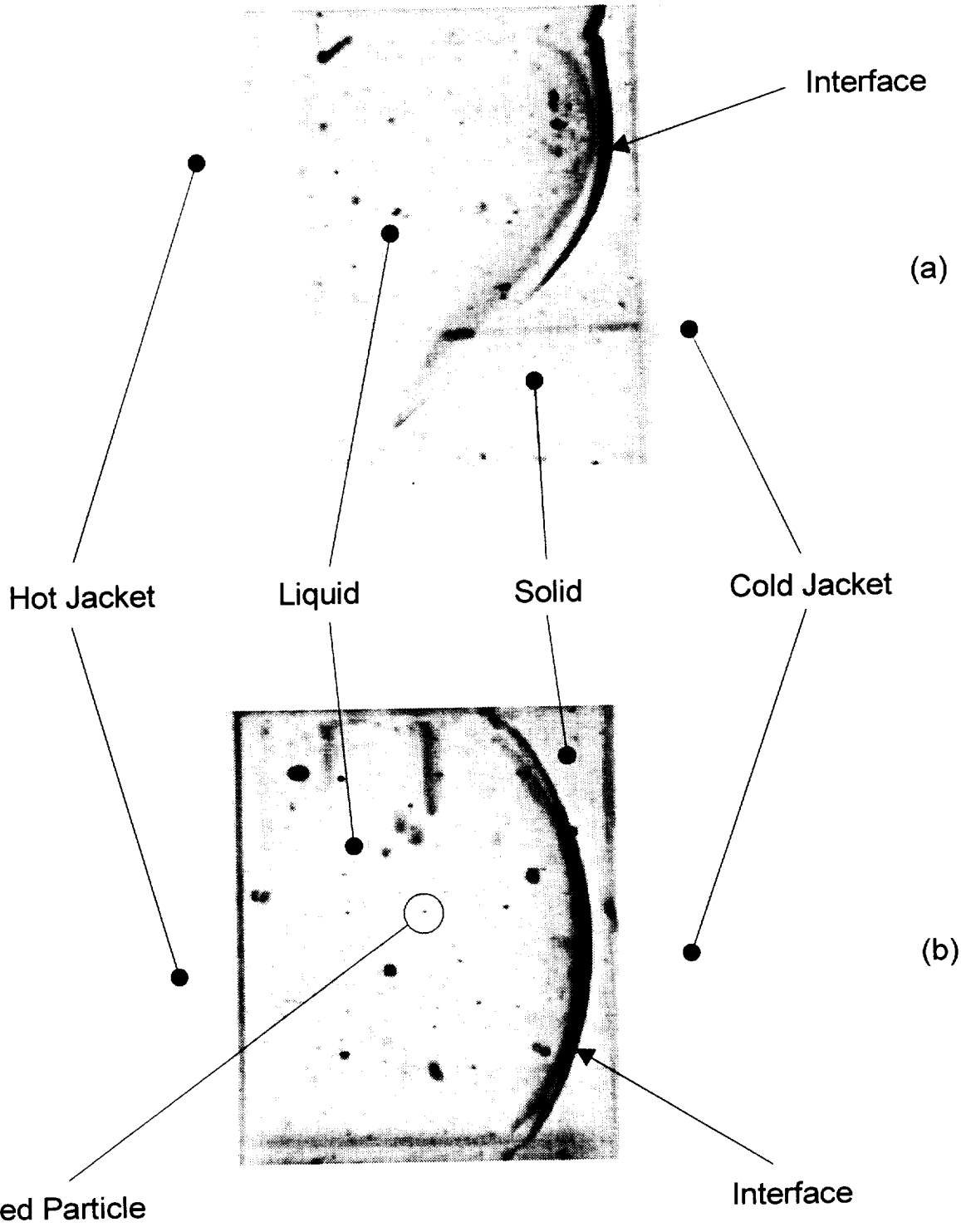

Figure 3. Samples of the images used to estimate the flow velocities for the pure SCN no-growth case, (a) side view and (b) top view. For reproducibility, the images have been inverted so that dark becomes light and vice-versa. The larger blobs and streaks are reflections from defects in the glass, while the smaller dots are the seed particles. The interface locations in the mid planes can be clearly seen, as well as the edges of the hot and cold jackets.

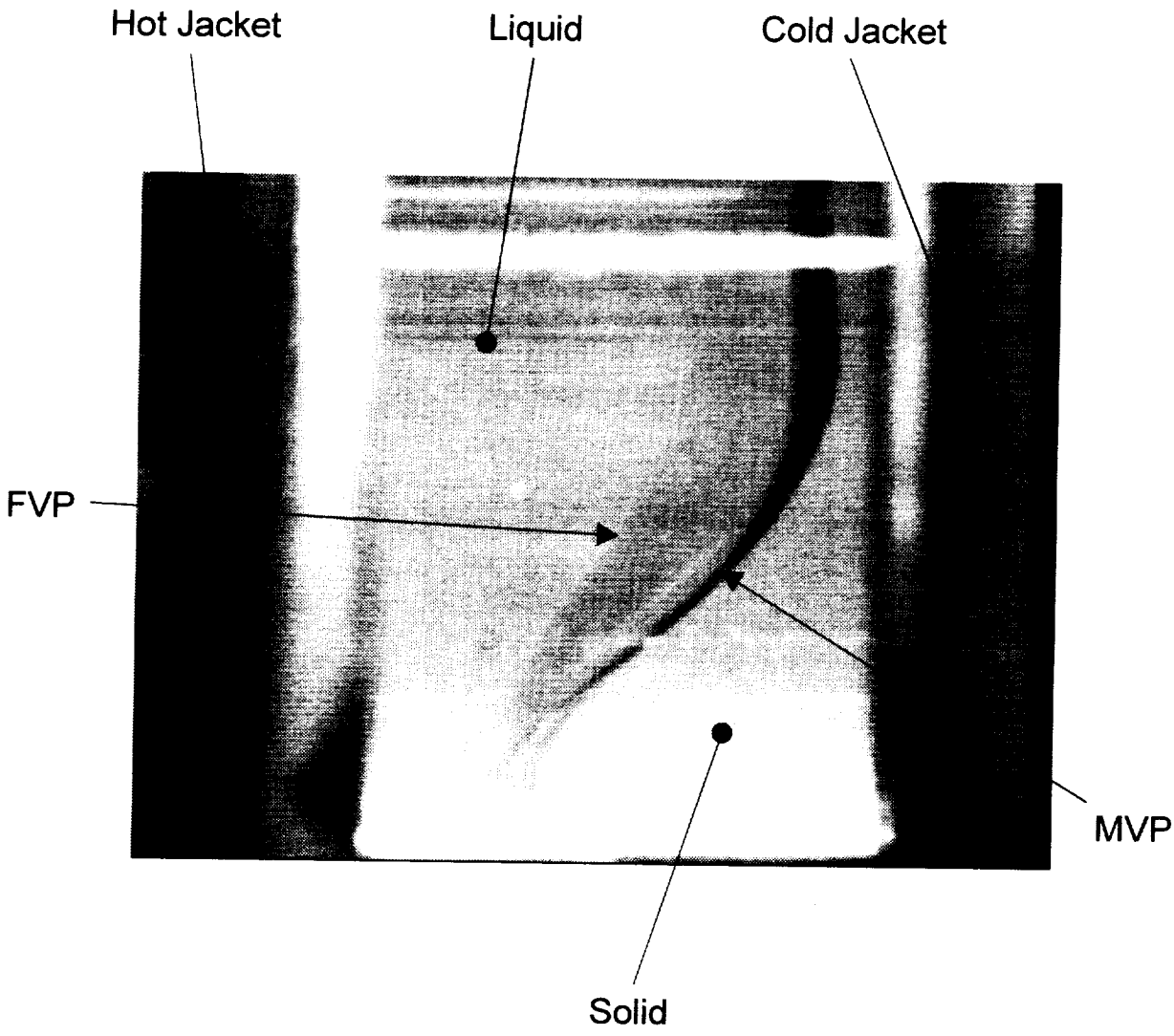

Figure 4. Sample of the images used to measure the solid/liquid interface. This image was captured from the horizontal camera and shows the interface in y-z planes. The case shown here is for pure SCN under no-growth conditions. The interface in the mid-vertical plane (MVP) and front-vertical plane (FVP) can be seen, as can the edges of the hot and cold jackets. Measurements taken from this image are shown in figure 7(a) and listed in table C.1(a).

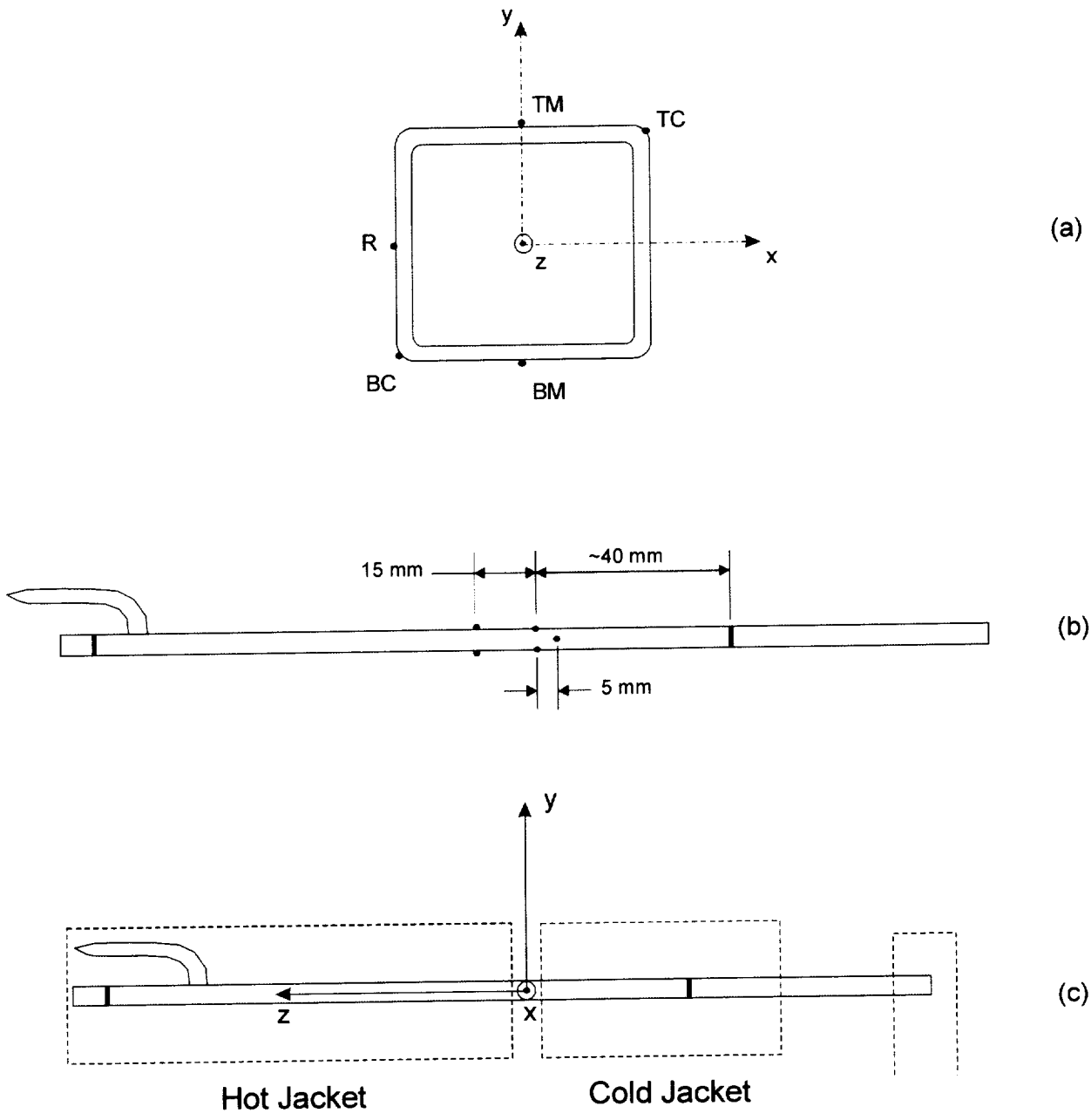

Figure 5. Schematics of ampoule instrumentation: (a) cross-section of ampoule showing thermocouple locations and definition for x-y coordinates, (b) pure SCN ampoule instrumented with five thermocouples and (c) schematic of ampoule mounted in furnace; z = 0 is taken to be in the center of the gap between the hot and cold jackets.

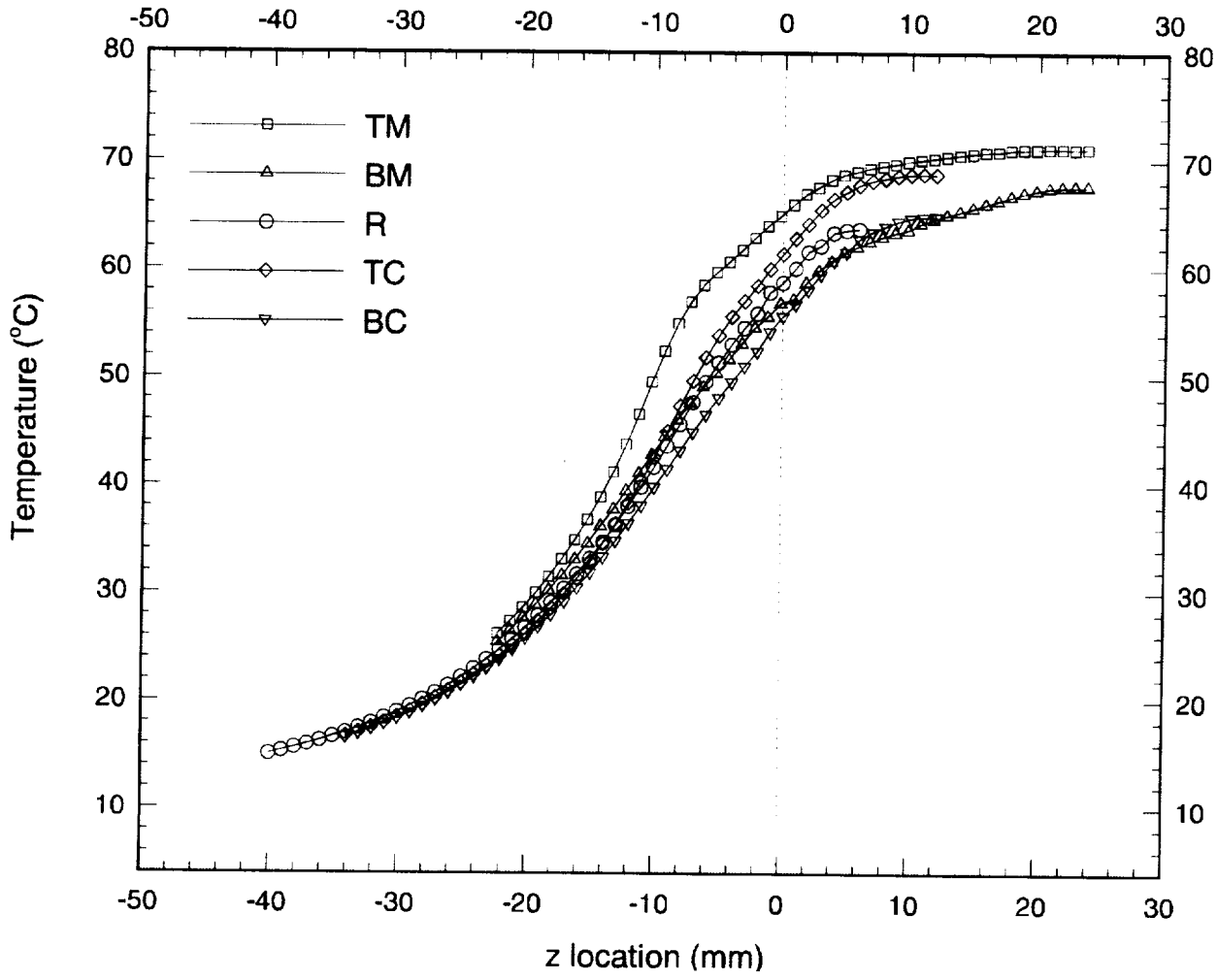

Figure 6. Temperature profiles for pure SCN at a growth rate of 40 μm/s. The locations of each thermocouple are indicated in Figure 5. The z = 0 position corresponds to the center of the 5 mm gradient zone. The thermocouple placed on top of the ampoule (TM) records the highest temperature for all locations; melt convection continually feeds warm fluid into this region and solid is melted back. The converse applies to the thermocouples mounted on the bottom of the ampoule (BM and BC).

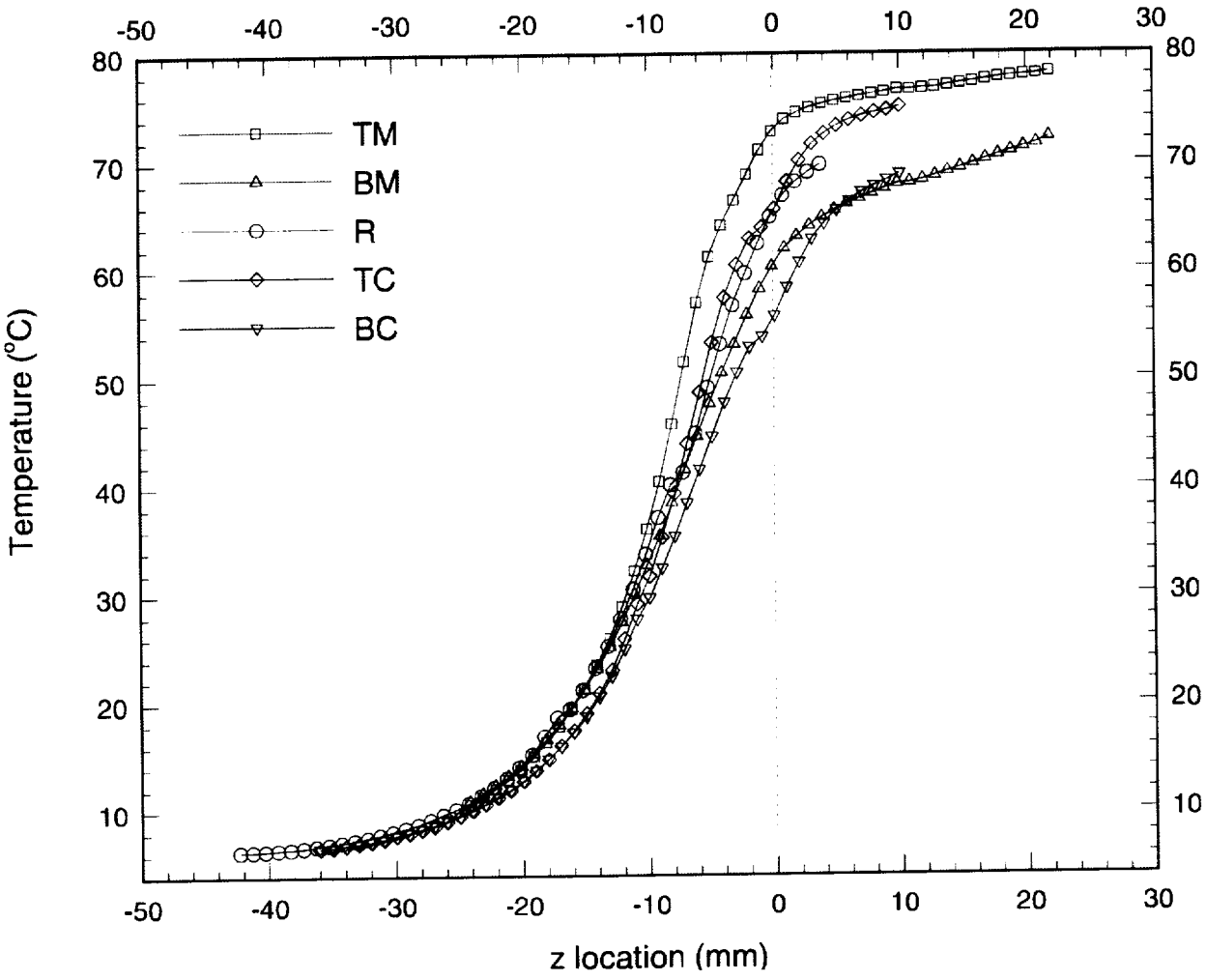

Figure 7. Temperature profiles for pure SCN at a growth rate of 2 μm/s. Thermocouple locations are indicated on Figure 5. The z = 0 location is in the center of the 1 mm gradient zone between the hot and cold furnaces. The most important detail to note is the increased thermal gradients detected by all thermocouples when compared to the case shown in Figure 6. This increased gradient assists the suppression of interface instability.

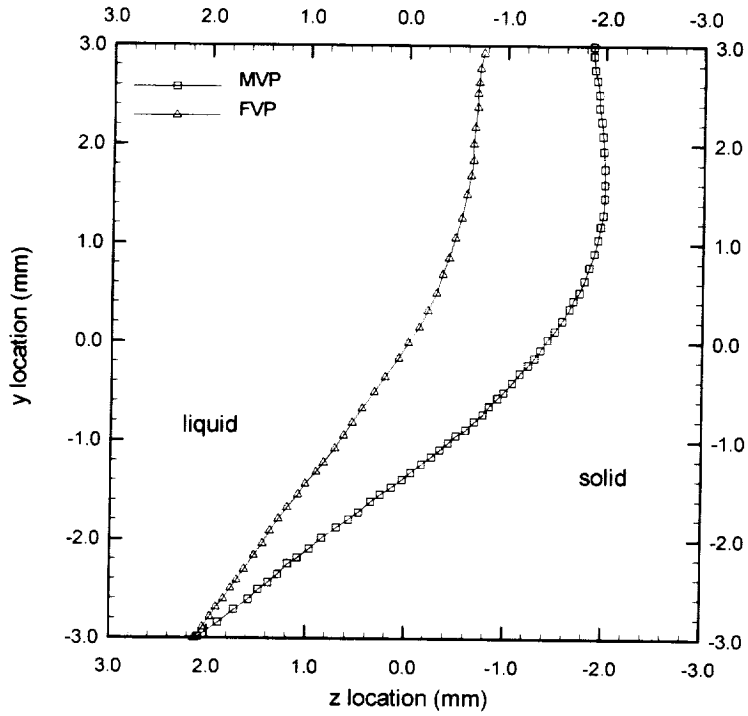

(a)

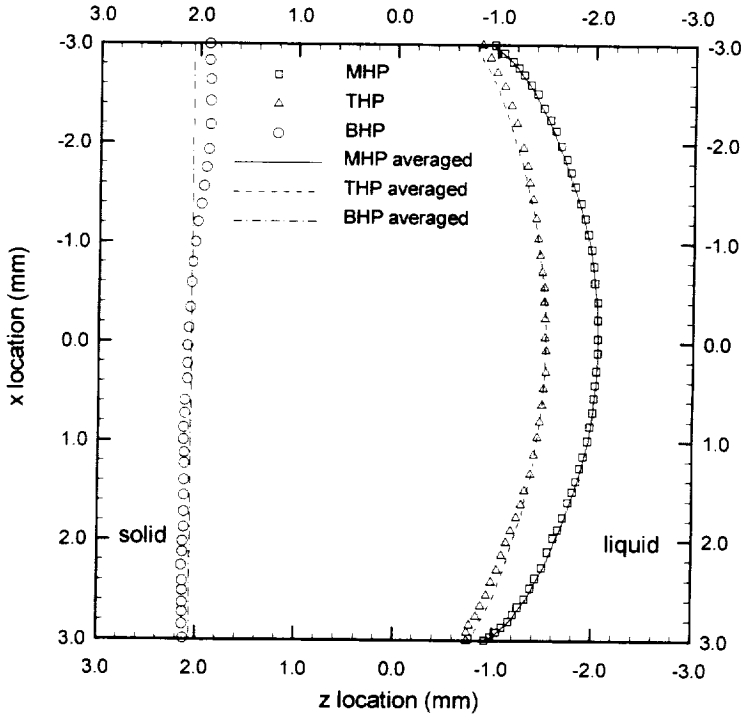

(b)

Figure 8. Front locations for pure SCN under no-growth conditions in (a) vertical planes and (b) horizontal planes. The interface is stable and non-dendritic but not planar, rather it is noticeably distorted from the vertical. The solid is concave with a symmetric crescent-like section when viewed from above and asymmetric and thicker towards the bottom when viewed from the side. The ordinates x = -3 and +3 correspond to the front and back walls, respectively while y = -3 and +3 correspond to the top and bottom walls, respectively.

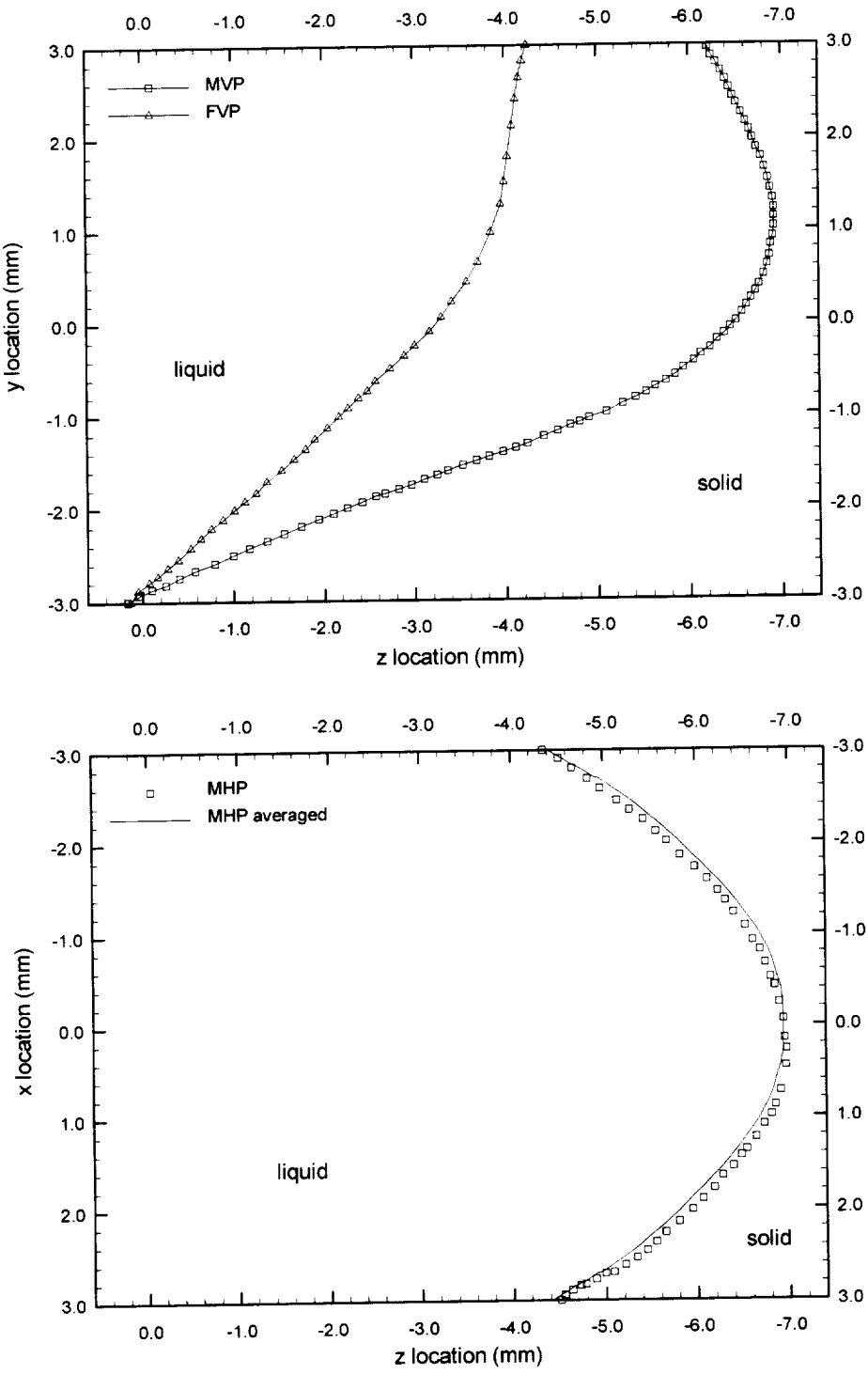

Figure 9. Front locations for pure SCN at a growth rate of 40 μm/s in (a) vertical planes and (b) horizontal planes. Translation of the jackets has led to an elongation of the interface in z, the difference between the minimum and maximum z locations has increased to 7.10 mm from 3.92 mm for the no-growth case (Figure 8). The solid also appears more concave when viewed from above than for the no-growth case.

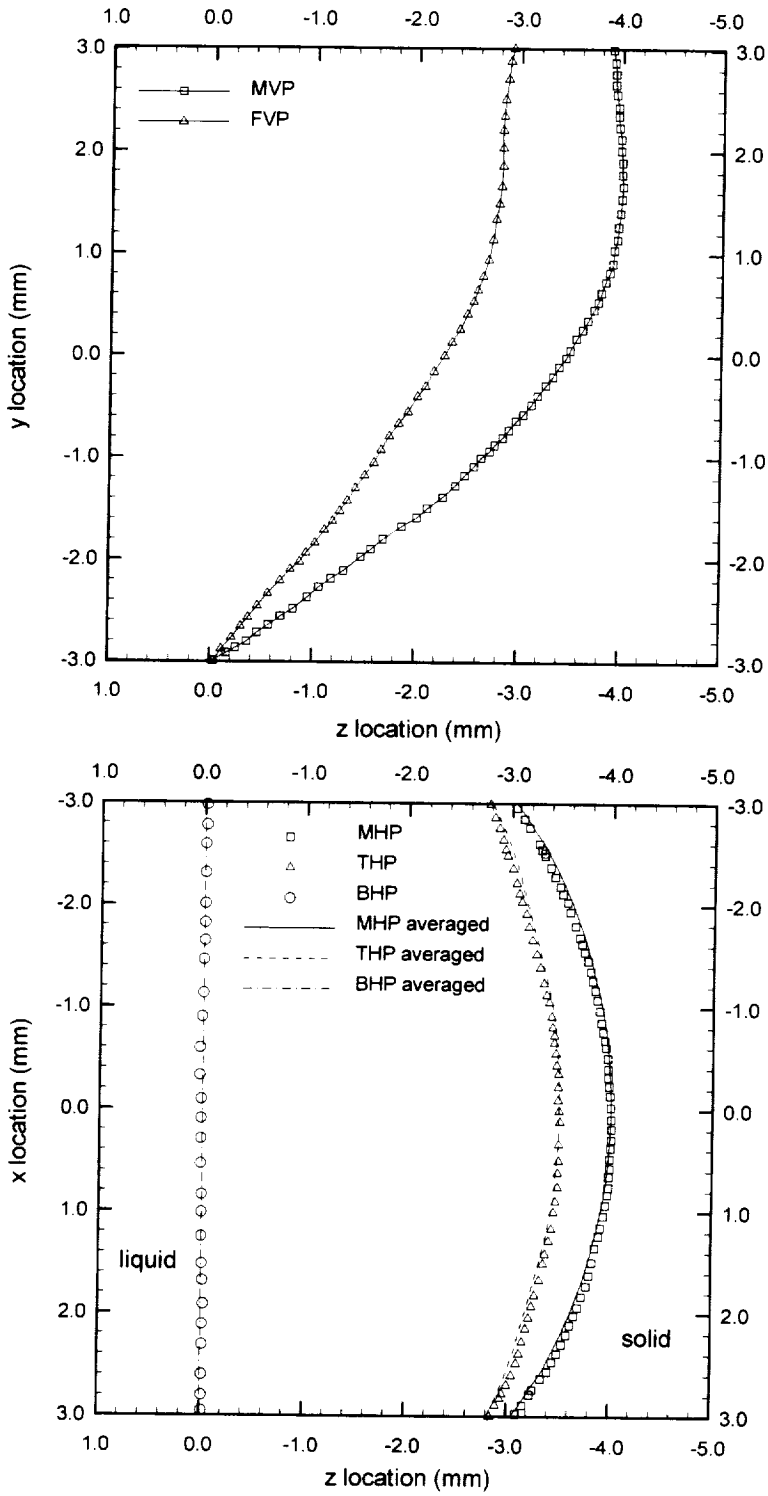

Figure 10. Front locations for pure SCN at a growth rate of 2 μm/s in (a) vertical planes and (b) horizontal planes. The temperature difference between hot and cold zones has been increased and the length of the gradient zone decreased when compared to the pure SCN no-growth case. This has led to a more compact interface shape than for the no-growth case, even though the jackets are moving.

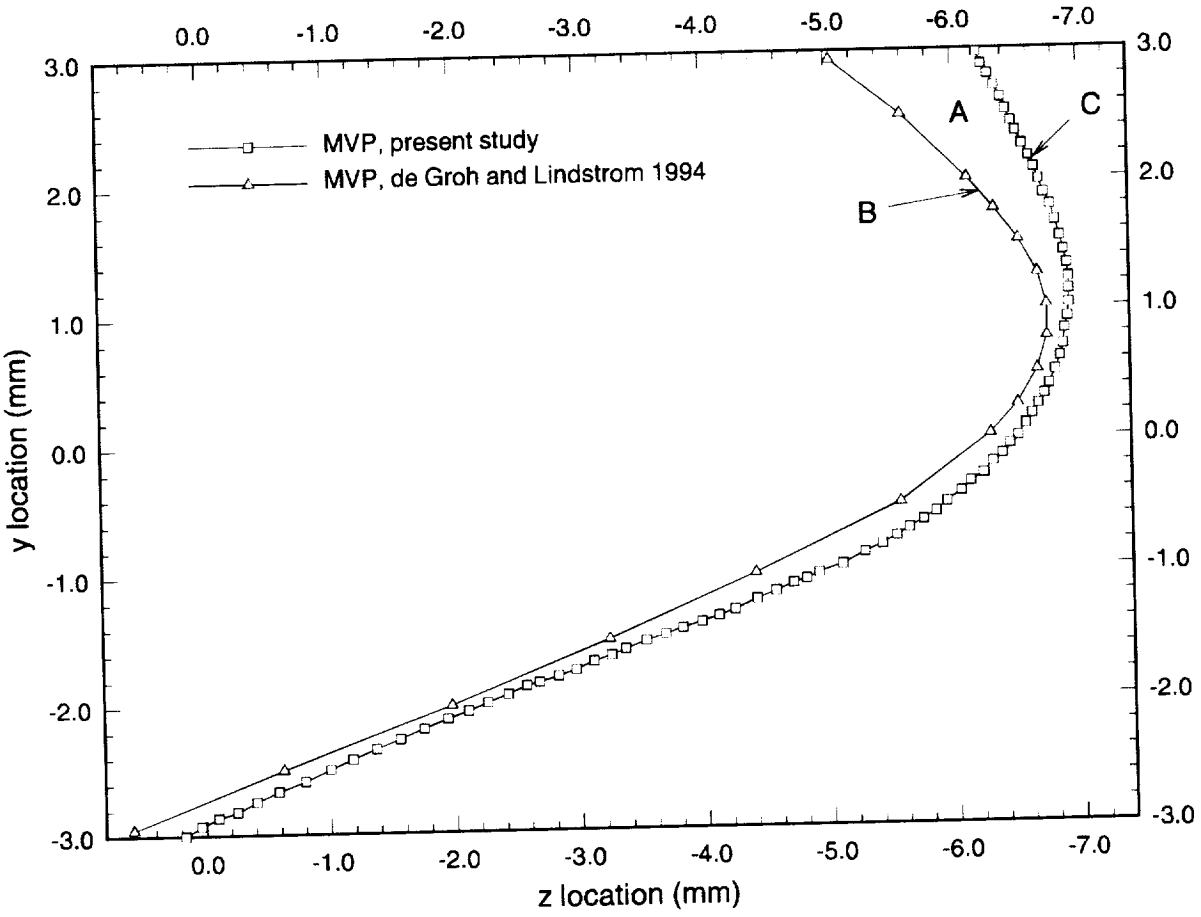

Figure 11. Comparison of interface shapes in the mid-vertical plane (MVP). Data is for pure SCN solidification at a growth rate of 40 μm/s, both from the present study and from de Groh and Lindstrom [2]. Review of SIV videotape indicates that particles, entrained in the liquid, travel through region "A" which suggests that the true interface passes through line "C" rather than line "B".

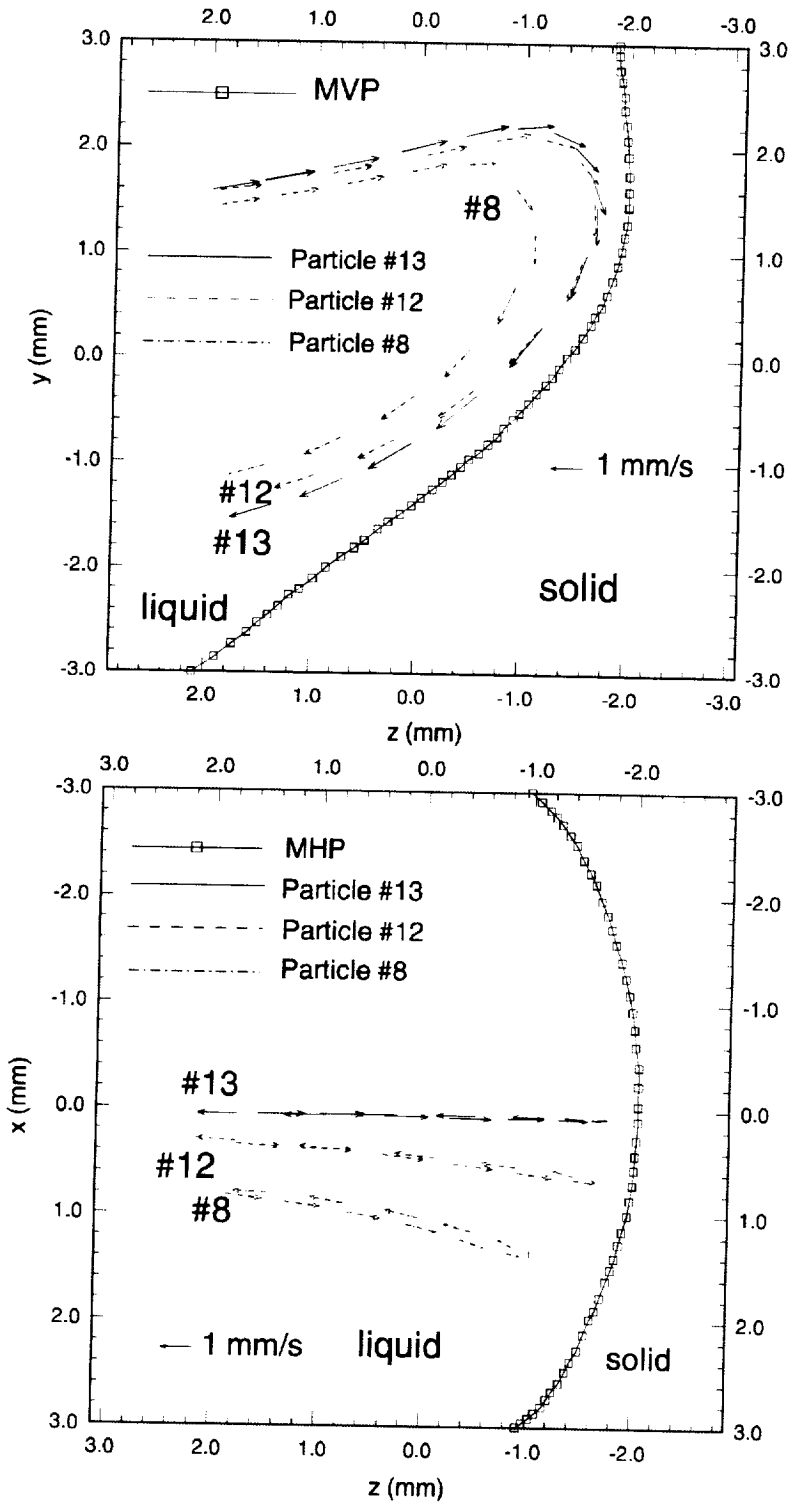

Figure 12. Plots of experimentally determined velocity values during no-growth for pure SCN in (a) vertical and (b) horizontal planes. The maximum velocity for particle #13 was found to be 1.50 ± 0.08 mm/s at (x, y, z) = (0.068, –0.3625, –0.567) mm. The vectors furnish an excellent description of the convective flow in the cavity.

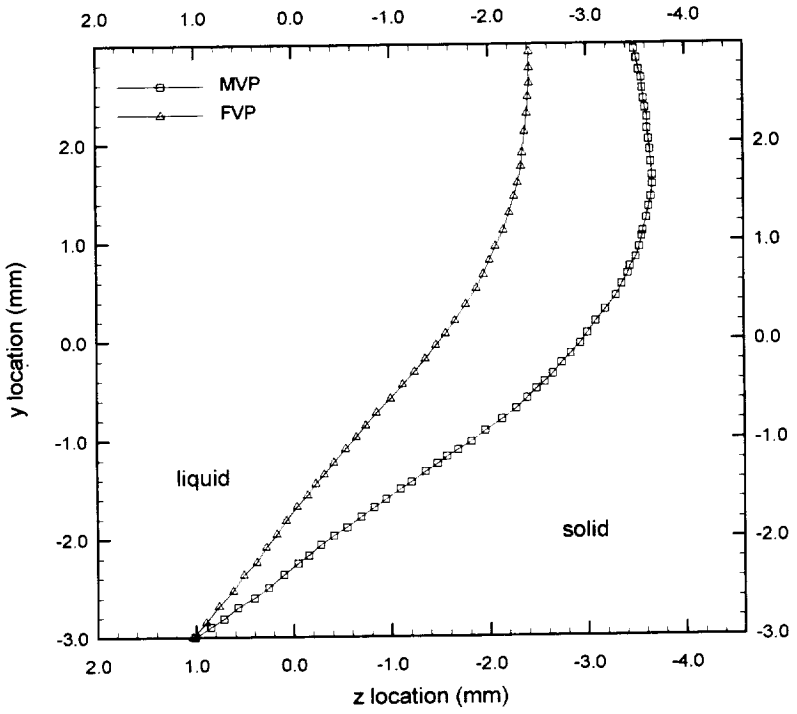

(a)

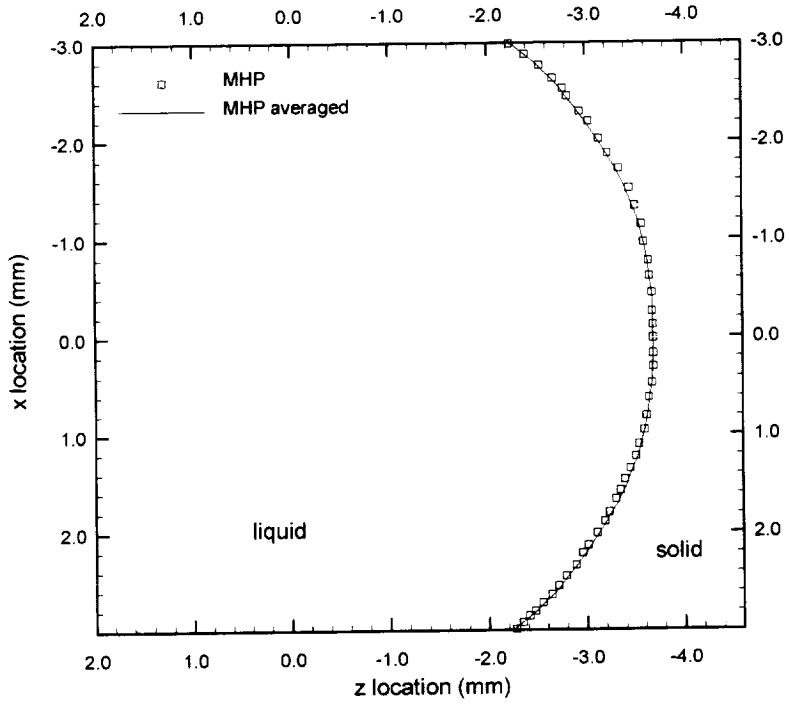

(b)

Figure 13. Front locations for SCN-ACE alloy under no-growth conditions in (a) vertical planes and (b) horizontal planes. The shape of the interface is remarkably similar to the results for the pure material under no-growth conditions (Figure 8); however, the minimum z location for the MVP is at –4.00 mm in this case, compared with –1.92 mm for the pure SCN. The lowering of the melting temperature by the inclusion of the alloying species is the cause of this repositioning of the interface

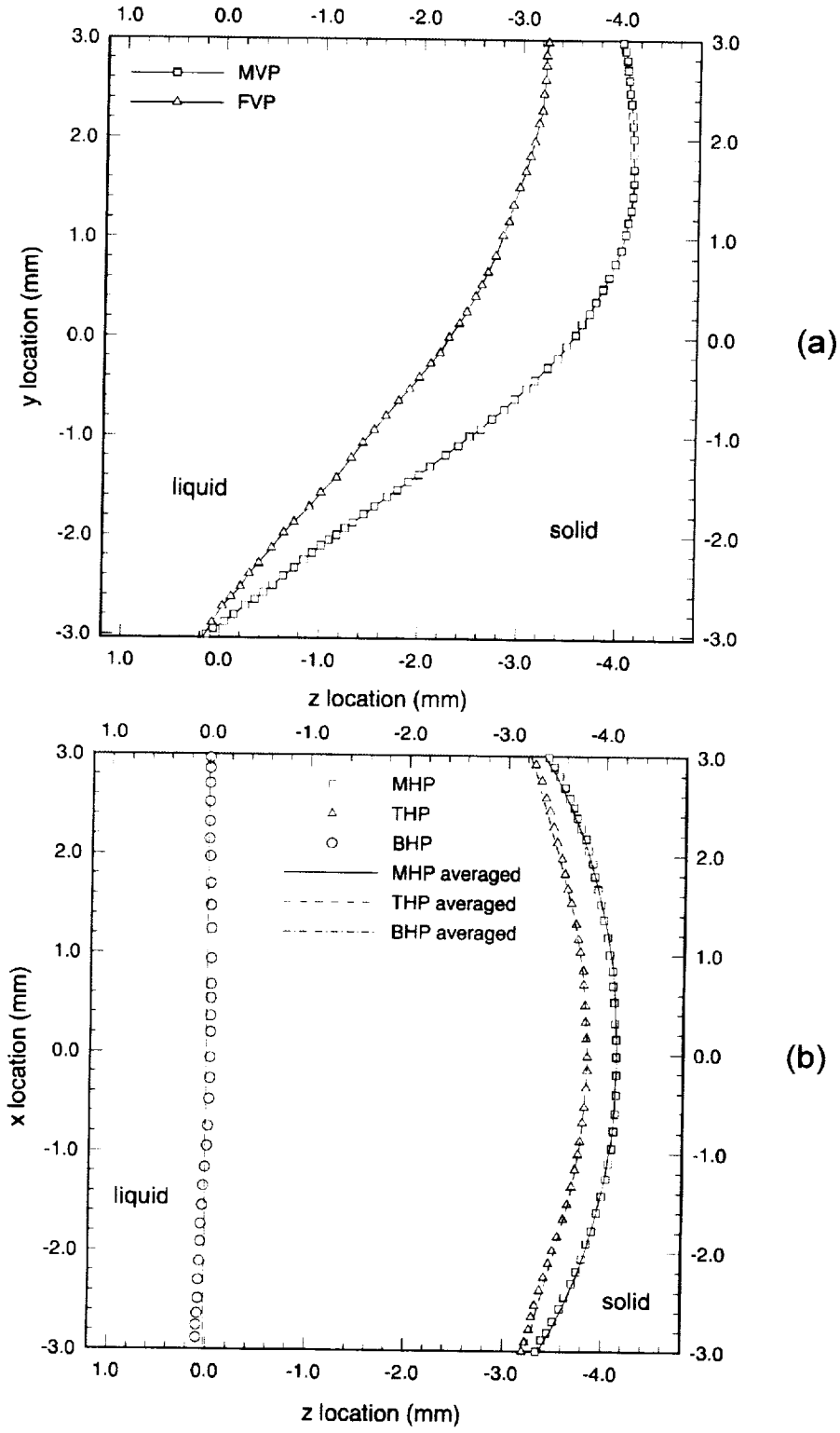

Figure 14. Front locations for SCN-ACE at a growth rate of 2 μm/s in (a) vertical planes and (b) horizontal planes. As for the alloy no-growth case (Figure 13), the shape of the interface is similar to the corresponding pure material case, but the interface is shifted back in z.

APPENDIX A - EQUIPMENT LIST[1]

To facilitate repeatability of the experiments performed in the present study, a table of the electronic equipment used to obtain flow visualization images and interface location data is provided below.

Item Description	Qty.	Model number	Manufacturer
High resolution B&W CCD-IRIS cameras	2	SSC-M370	Sony
B&W video monitor	1	-	Sony
B&W video monitor	1	-	Panasonic
Digital video tape recorder	2	DSR-30	Sony
Digital laser video disc recorder	2	LVR-3000AN	Sony
35 mm camera	1	OM-1N	Olympus
Data acquisition system	1	-	Hewlett-Packard
18-180 mm F/2.5 zoom lenses for CCD cameras	2	-	Navitar
Polarized fiber optic light source	2	DCR II	Fostec

Properties of succinonitrile (SCN, $(NC(CH_2)_2CN)$), succinonitrile-acetone alloy, and the borosilicate ampoule; molecular wt. is 80.092g/mol.

Property	SCN Liquid	SCN Solid	Ampoule	SCN-ACE
*Density at T_m, kg/m^3	985	1016	2300	
Thermal conductivity, W/mK	0.223	0.225	1.2	
Heat capacity, J/kgK	2000	1955	753.5	
*Thermal expansivity, β_T, K^{-1}	8.0×10^{-4}			2.5×10^{-3}
*Solutal expansivity, β_c, $wt\%^{-1}$				
Kinematic viscosity, m^2/s	2.6×10^{-6}			
Melting temperature, T_m, K		331.34		
Index of refraction	1.4172	1.4320		
Heat of fusion, J/g	47.			

[1]NASA does not endorse commercial products. Details about the products named in this paper were included for completeness and accuracy. No endorsement or criticism of these products by NASA should be assumed.

Property	SCN Liquid	SCN Solid	Ampoule	SCN-ACE
Entropy of fusion, J/gK	0.142			
Molar volume at T_m, cm^3	82.54	78.83		
Liquidus slope, K/mol%				2.17
Solidus slope, K/mol%				20
Partition coeficient, mol%/mol%				0.11

* The liquid density and thermal and solutal expansivities of SCN-ACE alloys at various temperatures are:

$$\rho_l = [(-3.04\text{x}10^{-6}\text{C}) - 7.810\text{x}10^{-4}]\text{T} + [(-1.40\text{x}10^{-5}\text{C}^2) - (2.114\text{x}10^{-3}\text{C}) + 1.0334]$$

$$\beta_T = -\frac{1}{\rho_l}\frac{\partial \rho_l}{\partial \text{T}} = \frac{3.04\text{x}10^{-6}\text{C} + 7.810\text{x}10^{-4}}{[(-3.04\text{x}10^{-6}\text{C}) - 7.810\text{x}10^{-4}]\text{T} + [(-1.40\text{x}10^{-5}\text{C}^2) - (2.114\text{x}10^{-3}\text{C}) + 1.0334]}$$

$$\beta_C = -\frac{1}{\rho_l}\frac{\partial \rho_l}{\partial \text{C}} = \frac{3.04\text{x}10^{-6}\text{T} + 2.81\text{x}10^{-5}\text{C} + 2.114\text{x}10^{-3}}{[(-3.04\text{x}10^{-6}\text{C}) - 7.810\text{x}10^{-4}]\text{T} + [(-1.40\text{x}10^{-5}\text{C}^2) - (2.114\text{x}10^{-3}\text{C}) + 1.0334]}$$

where ρ_l is in g/cm^3, C is in wt%, and T is in °C. These correlations are valid for acetone concentrations of 0 to 18 wt% and temperatures from the liquidus temperature to at least 30 °C above liquidus.

APPENDIX B - TEMPERATURE DATA

Thermocouple locations given in figure 5. z locations are in mm, temperatures are in °C.

Table B.1. Averaged temperature data for two pure SCN, growth runs at 40 μm/s.

z	TM	BM	z	R	z	TC	BC
23.7813	71.2840	67.7350	5.9702	64.6350	11.9864	68.9015	65.0190
22.7813	71.2720	67.7350	4.9702	64.6590	10.9864	68.9135	65.0190
21.7813	71.2840	67.7225	3.9702	64.4660	9.9864	68.8895	64.9230
20.7813	71.2965	67.6265	2.9702	63.8180	8.9864	68.7810	64.6585
19.7813	71.2720	67.4340	1.9702	63.2660	7.9864	68.6125	64.2620
18.7813	71.2355	67.1935	0.9702	62.1380	6.9864	68.3845	63.7820
17.7813	71.1635	66.8690	-0.0298	60.7950	5.9864	68.0475	63.0980
16.7813	71.0555	66.5085	-1.0298	59.3320	4.9864	67.5425	62.1980
15.7813	70.9710	66.1840	-2.0298	58.3980	3.9864	66.9175	61.3465
14.7813	70.8385	65.8240	-3.0298	57.1040	2.9864	66.0280	60.1355
13.7813	70.7065	65.4750	-4.0298	55.5240	1.9864	64.9230	58.9370
12.7813	70.5615	65.1510	-5.0298	53.8740	0.9864	63.6860	57.7390
11.7813	70.4175	64.7670	-6.0298	52.1290	-0.0136	62.2700	56.3860
10.7813	70.2485	64.3820	-7.0298	50.3130	-1.0136	60.8665	55.0220
9.7813	70.1045	63.8540	-8.0298	48.3740	-2.0136	59.4045	53.6110
8.7813	69.8995	63.5420	-9.0298	46.3010	-3.0136	57.9665	52.2480
7.7813	69.7075	63.1220	-10.0298	44.2050	-4.0136	56.5295	50.8030
6.7813	69.5025	62.6540	-11.0298	42.1360	-5.0136	54.9265	49.3275
5.7813	69.2505	62.2100	-12.0298	40.1420	-6.0136	53.0730	47.8220
4.7813	68.9615	61.6940	-13.0298	38.2470	-7.0136	50.9700	46.2275
3.7813	68.5765	60.9625	-14.0298	36.4520	-8.0136	48.6820	44.5385
2.7813	68.0350	60.2555	-15.0298	34.7550	-9.0136	46.3135	42.8385
1.7813	67.4220	59.2245	-16.0298	33.1810	-10.0136	43.9100	41.1150
0.7813	66.5450	58.0985	-17.0298	31.7050	-11.0136	41.6190	39.3795
-0.2187	65.5715	57.2960	-18.0298	30.3280	-12.0136	39.4165	37.6815
-1.2187	64.6105	56.1705	-19.0298	29.0240	-13.0136	37.3745	36.0090
-2.2187	63.4580	55.2970	-20.0298	27.7930	-14.0136	35.4805	34.4230
-3.2187	62.2460	54.0770	-21.0298	26.6850	-15.0136	33.7220	32.8980
-4.2187	61.0585	52.7620	-22.0298	25.6260	-16.0136	32.0865	31.4715
-5.2187	60.0155	51.6150	-23.0298	24.6410	-17.0136	30.5990	30.1315
-6.2187	58.8410	50.3015	-24.0298	23.7290	-18.0136	29.2085	28.8515
-7.2187	57.4040	48.9135	-25.0298	22.8660	-19.0136	27.9285	27.6455
-8.2187	55.5725	47.4800	-26.0298	22.0770	-20.0136	26.7470	26.5375
-9.2187	53.2280	45.9440	-27.0298	21.3120	-21.0136	25.6390	25.4660
-10.2187	50.4925	44.2920	-28.0298	20.6450	-22.0136	24.6040	24.4930
-11.2187	47.5720	42.6045	-29.0298	20.0030	-23.0136	23.6550	23.5690
-12.2187	44.6985	40.8685	-30.0298	19.3850	-24.0136	22.7670	22.7300

z	TM	BM	z	R	z	TC	BC
-13.2187	42.0375	39.1460	-31.0298	18.8410	-25.0136	21.9775	21.9410
-14.2187	39.6005	37.4605	-32.0298	18.2970	-26.0136	21.2255	21.2005
-15.2187	37.4115	35.8125	-33.0298	17.8270	-27.0136	20.5340	20.5215
-16.2187	35.4190	34.2265	-34.0298	17.3820	-28.0136	19.8795	19.8670
-17.2187	33.5745	32.7260	-35.0298	16.9610	-29.0136	19.2735	19.2490
-18.2187	31.9270	31.2875	-36.0298	16.5650	-30.0136	18.7050	18.6930
-19.2187	30.3895	29.9220	-37.0298	16.1940	-31.0136	18.1860	18.1610
-20.2187	28.9870	28.6545	-38.0298	15.8720	-32.0136	17.7040	17.7160
-21.2187	27.6950	27.4485	-39.0298	15.5500	-33.0136	17.2460	17.2460
-22.2187	26.5010	26.3160	-40.0298	15.2270	-34.0136	16.8250	16.8375

Table B.2. Temperature data for pure SCN, growth at 2 μm/s.

z	TM	BM	z	R	z	TC	BC
21.8233	78.1680	72.1150	3.6955	69.6830	10.0283	75.0550	68.8650
20.8233	77.9990	71.5610	2.6955	68.9850	9.0283	74.7180	68.2640
19.8233	77.9020	71.2240	1.6955	68.1190	8.0283	74.5010	67.7590
18.8233	77.8060	70.8630	0.6955	66.8450	7.0283	74.2110	67.1580
17.8233	77.6850	70.5020	-0.3045	64.8990	6.0283	73.8020	66.3640
16.8233	77.5160	70.1400	-1.3045	62.4260	5.0283	73.2710	65.4990
15.8233	77.3230	69.7310	-2.3045	59.6680	4.0283	72.5490	64.2980
14.8233	77.1540	69.3700	-3.3045	56.7210	3.0283	71.6090	62.8340
13.8233	77.0090	69.0090	-4.3045	53.1320	2.0283	70.0920	60.6990
12.8233	76.8160	68.6010	-5.3045	49.1430	1.0283	68.1440	58.3980
11.8233	76.7200	68.2640	-6.3045	44.8710	0.0283	65.6190	55.7640
10.8233	76.6230	68.0470	-7.3045	41.2990	-0.9717	63.8900	53.8260
9.8233	76.6470	67.9270	-8.3045	40.1420	-1.9717	62.8820	52.8930
8.8233	76.4060	67.4700	-9.3045	37.1160	-2.9717	60.4590	50.5040
7.8233	76.2130	67.0370	-10.3045	33.7220	-3.9717	57.4400	47.7820
6.8233	76.0200	66.5330	-11.3045	30.5000	-4.9717	53.2760	44.6240
5.8233	75.8270	66.0520	-12.3045	27.7440	-5.9717	48.6900	41.5940
4.8233	75.5860	65.4750	-13.3045	25.2320	-6.9717	43.9340	38.4940
3.8233	75.3200	64.8270	-14.3045	23.2110	-7.9717	39.3550	35.3940
2.8233	74.9830	64.0580	-15.3045	21.1880	-8.9717	35.2710	32.4680
1.8233	74.5250	63.0980	-16.3045	19.4350	-9.9717	31.7050	29.7370
0.8233	73.8980	61.9940	-17.3045	18.6680	-10.9717	29.1720	27.7440
-0.1768	72.7890	60.2910	-18.3045	16.9370	-11.9717	25.9220	25.0110
-1.1768	71.0550	58.2300	-19.3045	15.2270	-12.9717	23.0390	22.4710
-2.1768	68.8170	55.8590	-20.3045	14.0870	-13.9717	20.9170	20.5710
-3.1768	66.4370	53.1320	-21.3045	13.0690	-14.9717	19.0140	18.7920
-4.1768	64.1060	50.4800	-22.3045	12.1990	-15.9717	17.4320	17.3330
-5.1768	61.2020	47.6580	-23.3045	11.4530	-16.9717	16.0450	15.9960
-6.1768	56.9610	44.6240	-24.3045	10.7570	-17.9717	14.8060	14.8310

z	TM	BM	z	R	z	TC	BC
-7.1768	51.5070	41.5700	-25.3045	10.1840	-18.9717	13.7390	13.8140
-8.1768	45.7830	38.4940	-26.3045	9.6860	-19.9717	12.7710	12.8450
-9.1768	40.4620	35.4440	-27.3045	9.1880	-20.9717	11.9260	12.0000
-10.1767	36.0830	32.7140	-28.3045	8.7640	-21.9717	11.2790	11.3790
-11.1767	32.2220	29.9840	-29.3045	8.4390	-22.9717	10.6320	10.7070
-12.1767	28.8760	27.4730	-30.3045	8.0900	-23.9717	10.0600	10.1090
-13.1767	25.9710	25.1580	-31.3045	7.8150	-24.9717	9.5360	9.5860
-14.1767	23.5320	23.1370	-32.3045	7.5660	-25.9717	9.0630	9.1380
-15.1767	21.3360	21.2130	-33.3045	7.3410	-26.9717	8.6390	8.7140
-16.1767	19.4590	19.5330	-34.3045	7.1410	-27.9717	8.3150	8.3650
-17.1767	17.8030	18.0010	-35.3045	6.9660	-28.9717	7.9900	8.0400
-18.1767	16.3920	16.6390	-36.3045	6.8160	-29.9717	7.7410	7.7650
-19.1767	15.0540	15.3270	-37.3045	6.6910	-30.9717	7.4410	7.4660
-20.1767	13.8630	14.1860	-38.3045	6.5660	-31.9717	7.2160	7.2410
-21.1767	12.9200	13.2180	-39.3045	6.4910	-32.9717	7.0160	7.0660
-22.1767	12.0750	12.3980	-40.3045	6.4160	-33.9717	6.8660	6.8910
-23.1767	11.3290	11.6280	-41.3045	6.3660	-34.9717	6.7160	6.7410
-24.1767	10.6570	10.9560	-42.3045	6.3160	-35.9717	6.6160	6.6160

APPENDIX C - INTERFACE SHAPES

Note that the abbreviations used for the interface planes do not match those in [2]. Values in mm.

Table C.1(a). Interface shapes for pure SCN, no growth, vertical planes.

z	y, MVP	z	y, FVP
2.0946	-2.9857	2.1315	-3.0000
1.8857	-2.8426	2.0455	-2.8903
1.7260	-2.7114	1.9717	-2.7830
1.5786	-2.6041	1.9103	-2.6876
1.4803	-2.5087	1.8366	-2.6041
1.3821	-2.4372	1.7629	-2.4968
1.2838	-2.3537	1.7015	-2.4133
1.1855	-2.2464	1.6278	-2.3060
1.0872	-2.1868	1.5295	-2.1629
0.9644	-2.0914	1.4435	-2.0437
0.8415	-1.9841	1.3698	-1.9125
0.6941	-1.8768	1.2838	-1.7933
0.5713	-1.7933	1.1978	-1.6741
0.4730	-1.7218	1.0872	-1.5429
0.3501	-1.6144	1.0135	-1.4356
0.2518	-1.5429	0.9029	-1.3164
0.1413	-1.4714	0.8292	-1.2210
0.0307	-1.3879	0.7187	-1.0779
-0.0553	-1.3164	0.6327	-0.9467
-0.1659	-1.2329	0.5467	-0.8156
-0.2641	-1.1613	0.4484	-0.6725
-0.3501	-1.0898	0.3256	-0.5055
-0.4361	-1.0183	0.2150	-0.3505
-0.5098	-0.9467	0.0799	-0.1598
-0.6081	-0.8871	-0.0184	-0.0048
-0.6941	-0.8036	-0.1290	0.1503
-0.7801	-0.7321	-0.2150	0.3172
-0.8415	-0.6486	-0.3010	0.4960
-0.9275	-0.5652	-0.3624	0.6868
-0.9889	-0.5055	-0.4238	0.8537
-1.0749	-0.4102	-0.4853	1.0565
-1.1487	-0.3148	-0.5467	1.2592
-1.2346	-0.2313	-0.5958	1.4976
-1.2961	-0.1598	-0.6327	1.6884
-1.3575	-0.0763	-0.6573	1.8434
-1.4312	0.0310	-0.6573	2.0103
-1.5049	0.1145	-0.6695	2.1773

z	y, MVP	z	y, FVP
-1.5786	0.2218	-0.6941	2.3800
-1.6523	0.3410	-0.6941	2.5231
-1.6892	0.4245	-0.7064	2.6304
-1.7506	0.5080	-0.7187	2.7735
-1.7998	0.6272	-0.7555	2.9285
-1.8489	0.7584		
-1.8980	0.9014		
-1.9349	1.0445		
-1.9595	1.1757		
-1.9840	1.2949		
-1.9963	1.4619		
-1.9963	1.6049		
-1.9963	1.7599		
-1.9840	1.9388		
-1.9717	2.0938		
-1.9595	2.2369		
-1.9349	2.3800		
-1.9349	2.5111		
-1.9103	2.6542		
-1.8858	2.7615		
-1.8735	2.9046		
-1.8735	3.0000		

Table C.1(b). Interface shapes for pure SCN, no growth, horizontal planes.

z	x, MHP	z	x, THP	z	x, BHP
-0.9455	3.0000	-0.7599	3.0000	2.1636	2.9880
-1.0035	2.9641	-0.7599	2.9162	2.1752	2.8443
-1.0615	2.9162	-0.7831	2.8443	2.1752	2.7246
-1.1195	2.8683	-0.8527	2.7605	2.1752	2.6287
-1.1891	2.8084	-0.8991	2.6527	2.1752	2.5090
-1.2355	2.7365	-0.9571	2.5449	2.1752	2.4132
-1.2819	2.6647	-1.0035	2.4132	2.1868	2.2575
-1.3515	2.5808	-1.0615	2.2934	2.1752	2.1257
-1.4095	2.4731	-1.1079	2.1497	2.1752	2.0180
-1.4559	2.3772	-1.1543	2.0180	2.1636	1.8743
-1.5255	2.2695	-1.2007	1.8982	2.1636	1.7186
-1.5835	2.1138	-1.2587	1.7665	2.1636	1.5509
-1.6415	1.9701	-1.3051	1.6347	2.1636	1.3952
-1.6879	1.8862	-1.3399	1.4910	2.1636	1.2275
-1.7343	1.7665	-1.3979	1.3234	2.1636	1.1198
-1.7923	1.6108	-1.4327	1.1317	2.1752	0.9880
-1.8388	1.5030	-1.4675	0.9521	2.1752	0.8683

z	x, MHP	z	x, THP	z	x, BHP
-1.8736	1.3952	-1.4907	0.7964	2.1636	0.7246
-1.9084	1.2635	-1.5139	0.6287	2.1636	0.5928
-1.9432	1.1437	-1.5255	0.4611	2.1404	0.3772
-1.9896	0.9880	-1.5487	0.2934	2.1404	0.2216
-2.0128	0.8443	-1.5487	0.0778	2.1404	0.0419
-2.0360	0.7006	-1.5371	-0.0539	2.1288	-0.1377
-2.0476	0.5569	-1.5371	-0.2455	2.1172	-0.3413
-2.0592	0.4252	-1.5255	-0.4132	2.1056	-0.5928
-2.0708	0.2814	-1.5255	-0.5569	2.0940	-0.7964
-2.0824	0.1018	-1.5023	-0.7126	2.0708	-1.0000
-2.0824	-0.0419	-1.4791	-0.8802	2.0476	-1.2036
-2.0824	-0.2335	-1.4559	-1.0479	2.0128	-1.3832
-2.0824	-0.4132	-1.4327	-1.2515	1.9896	-1.5629
-2.0476	-0.6048	-1.3979	-1.4431	1.9664	-1.7545
-2.0360	-0.7725	-1.3631	-1.6108	1.9432	-1.9341
-2.0128	-0.9401	-1.3399	-1.7784	1.9316	-2.1856
-1.9780	-1.0958	-1.2935	-1.9581	1.9316	-2.4252
-1.9432	-1.2515	-1.2239	-2.2096	1.9316	-2.6407
-1.8968	-1.4072	-1.1659	-2.3892	1.9432	-2.8323
-1.8388	-1.5749	-1.0963	-2.5808	1.9432	-3.0000
-1.7923	-1.7186	-1.0151	-2.7246		
-1.7459	-1.8503	-0.9455	-2.8683		
-1.6879	-1.9820	-0.8643	-3.0000		
-1.6299	-2.1377				
-1.5719	-2.2455				
-1.5023	-2.3653				
-1.4327	-2.5090				
-1.3662	-2.5995				
-1.2935	-2.7006				
-1.2355	-2.7725				
-1.1775	-2.8323				
-1.0847	-2.9162				
-0.9919	-3.0000				

Table C.2(a) Interface shapes for pure SCN, 40 μm/s growth, vertical planes.

z	y, MVP	z	y, FVP
-6.2078	2.9695	0.1430	-3.0000
-6.2458	2.8782	0.0542	-2.8782
-6.2965	2.8020	-0.0725	-2.7868
-6.3472	2.7107	-0.1613	-2.7259
-6.3979	2.6193	-0.2753	-2.6345
-6.4360	2.5279	-0.3894	-2.5432

z	y, MVP	z	y, FVP
-6.4740	2.4365	-0.5289	-2.4213
-6.5120	2.3604	-0.6429	-2.3147
-6.5627	2.2538	-0.7570	-2.2081
-6.6134	2.1624	-0.8838	-2.1168
-6.6515	2.0711	-1.0106	-2.0102
-6.6895	1.9797	-1.1246	-1.9188
-6.7275	1.8731	-1.2514	-1.8274
-6.7782	1.7817	-1.3655	-1.7056
-6.8162	1.6599	-1.5303	-1.5838
-6.8543	1.5381	-1.6697	-1.4619
-6.8796	1.4315	-1.7965	-1.3553
-6.9050	1.3249	-1.8979	-1.2487
-6.9177	1.2183	-2.0373	-1.1269
-6.9177	1.1269	-2.1641	-1.0051
-6.9177	1.0203	-2.2655	-0.9137
-6.9050	0.9137	-2.3796	-0.8071
-6.8796	0.8223	-2.4810	-0.7310
-6.8669	0.7005	-2.5697	-0.6244
-6.8416	0.6091	-2.7345	-0.4873
-6.8036	0.5025	-2.8866	-0.3503
-6.7529	0.3959	-3.0007	-0.2437
-6.7148	0.3198	-3.1655	-0.0914
-6.6641	0.2437	-3.2923	0.0609
-6.6134	0.1675	-3.4064	0.2284
-6.5627	0.0914	-3.5711	0.4416
-6.4993	0.0000	-3.6979	0.6548
-6.4360	-0.0609	-3.8373	0.9746
-6.3726	-0.1371	-3.9514	1.2792
-6.2965	-0.1980	-3.9895	1.5228
-6.2205	-0.2893	-4.0275	1.7970
-6.1191	-0.3503	-4.0782	2.1320
-6.0430	-0.4264	-4.1162	2.4213
-5.9289	-0.5025	-4.1542	2.6497
-5.8402	-0.5787	-4.1923	2.8325
-5.7388	-0.6396	-4.2430	3.0000
-5.6247	-0.7005		
-5.5233	-0.7614		
-5.4092	-0.8223		
-5.2697	-0.8833		
-5.0923	-0.9746		
-4.9021	-1.0355		
-4.8007	-1.0812		
-4.6993	-1.1117		

z	y, MVP	z	y, FVP
-4.5599	-1.1726		
-4.4078	-1.2335		
-4.2303	-1.3096		
-4.1035	-1.3553		
-3.9641	-1.4010		
-3.8120	-1.4467		
-3.6726	-1.4924		
-3.5204	-1.5381		
-3.3556	-1.5990		
-3.2416	-1.6447		
-3.1021	-1.6904		
-2.9627	-1.7513		
-2.8232	-1.7970		
-2.6711	-1.8426		
-2.5697	-1.8694		
-2.4176	-1.9340		
-2.2528	-1.9949		
-2.1007	-2.0558		
-1.9359	-2.1168		
-1.7458	-2.1929		
-1.5556	-2.2690		
-1.3655	-2.3452		
-1.1753	-2.4213		
-0.9979	-2.4975		
-0.7951	-2.5888		
-0.5796	-2.6650		
-0.4021	-2.7411		
-0.2500	-2.8173		
-0.0979	-2.8629		
0.0416	-2.9239		
0.1683	-3.0000		

Table C.2(b) Interface shapes for pure SCN, 40 μm/s growth, horizontal planes.

z	x, MHP
-4.5094	3.0000
-4.5547	2.9408
-4.6339	2.8886
-4.7244	2.8364
-4.7810	2.8233
-4.8941	2.7711
-4.9959	2.7058
-5.0865	2.6927

z	x, MHP
-5.2109	2.6144
-5.3354	2.5361
-5.4485	2.4577
-5.5503	2.3663
-5.6522	2.2618
-5.7992	2.1443
-5.9463	2.0137
-6.0595	1.8962
-6.1839	1.7787
-6.2744	1.6481
-6.3876	1.5437
-6.4781	1.4262
-6.5347	1.3609
-6.6365	1.2303
-6.7270	1.0867
-6.8062	0.9822
-6.8515	0.8777
-6.9080	0.7210
-6.9646	0.4468
-6.9759	0.2640
-6.9533	0.1465
-6.9420	-0.0624
-6.8967	-0.2452
-6.8515	-0.4280
-6.8062	-0.5194
-6.7496	-0.6761
-6.6931	-0.8198
-6.6139	-0.9242
-6.5347	-1.0809
-6.4102	-1.2246
-6.3197	-1.3551
-6.2405	-1.4596
-6.1274	-1.5902
-5.9916	-1.7207
-5.8332	-1.8513
-5.6861	-2.0080
-5.5730	-2.1125
-5.4372	-2.2431
-5.2901	-2.3475
-5.1543	-2.4520
-4.9733	-2.5826
-4.8376	-2.6870
-4.6678	-2.8045

-4.5208	-2.9090
-4.3510	-3.0000

Table C.3(a) Interface shapes for pure SCN, 2 μm/s growth, vertical planes.

z	y, MVP	z	y, FVP
-0.0322	-2.9938	-0.0322	-3.0000
-0.1622	-2.9190	-0.1122	-2.8816
-0.2522	-2.8692	-0.2122	-2.7695
-0.3622	-2.8069	-0.3022	-2.6573
-0.4622	-2.7196	-0.3722	-2.5701
-0.5722	-2.6449	-0.4622	-2.4579
-0.6921	-2.5576	-0.5622	-2.3333
-0.8121	-2.4829	-0.6821	-2.2087
-0.9521	-2.3707	-0.7821	-2.0966
-1.0621	-2.2710	-0.8721	-2.0218
-1.1821	-2.1838	-0.9321	-1.9346
-1.3021	-2.1090	-1.0221	-1.8349
-1.4721	-1.9720	-1.1121	-1.7103
-1.5721	-1.8972	-1.1921	-1.6231
-1.6921	-1.7975	-1.2621	-1.5234
-1.8721	-1.6729	-1.3321	-1.4237
-2.0220	-1.5857	-1.4121	-1.2991
-2.1220	-1.4984	-1.5021	-1.1745
-2.2720	-1.3863	-1.5921	-1.0498
-2.3920	-1.2741	-1.6621	-0.9252
-2.4820	-1.1745	-1.7421	-0.7882
-2.5720	-1.0872	-1.8321	-0.6636
-2.6420	-1.0000	-1.9221	-0.5514
-2.7220	-0.9377	-2.0120	-0.4019
-2.7720	-0.8754	-2.0920	-0.3022
-2.8520	-0.8006	-2.1720	-0.1527
-2.9120	-0.7259	-2.2720	-0.0031
-2.9820	-0.6386	-2.3420	0.1340
-3.0520	-0.5763	-2.4220	0.2586
-3.1320	-0.4766	-2.4920	0.4081
-3.1920	-0.3894	-2.5520	0.5327
-3.2720	-0.2897	-2.5920	0.6449
-3.3420	-0.2025	-2.6420	0.7819
-3.4019	-0.1028	-2.6920	0.9439
-3.4719	-0.0156	-2.7320	1.1433
-3.5119	0.0592	-2.7620	1.3427
-3.5719	0.1713	-2.7920	1.4922
-3.6319	0.2586	-2.8120	1.6667

z	y, MVP	z	y, FVP
-3.6819	0.3458	-2.8220	1.8660
-3.7419	0.4579	-2.8220	2.0405
-3.7819	0.5327	-2.8220	2.2150
-3.8119	0.6199	-2.8320	2.3520
-3.8519	0.7321	-2.8420	2.5140
-3.8919	0.8193	-2.8720	2.7134
-3.9219	0.9065	-2.8920	2.8879
-3.9319	1.0436	-2.9220	3.0000
-3.9619	1.1433		
-3.9719	1.2679		
-3.9919	1.4050		
-4.0019	1.5421		
-4.0119	1.6667		
-4.0019	1.7788		
-4.0019	1.9034		
-3.9919	2.0156		
-3.9919	2.1277		
-3.9719	2.2399		
-3.9619	2.3520		
-3.9619	2.4393		
-3.9419	2.5639		
-3.9319	2.6636		
-3.9319	2.7632		
-3.9219	2.8754		
-3.9019	3.0000		

Table C.3(b) Interface shapes for pure SCN, 2 μm/s growth, horizontal planes.

z	x, MHP	z	x, THP	z	x, BHP
-3.0182	3.0000	-2.8364	3.0000	-0.0182	2.9533
-3.0909	2.9766	-2.8909	2.8949	-0.0182	2.8015
-3.1546	2.8949	-2.9364	2.8248	-0.0182	2.6029
-3.2273	2.7898	-2.9546	2.7781	-0.0182	2.3110
-3.2546	2.7431	-3.0000	2.6964	-0.0182	2.1124
-3.3364	2.6380	-3.0455	2.6029	-0.0273	1.9139
-3.4000	2.5679	-3.0909	2.4861	-0.0182	1.6803
-3.4455	2.4745	-3.1182	2.3927	-0.0091	1.5168
-3.4909	2.3927	-3.1455	2.2759	0.0000	1.2482
-3.5364	2.2993	-3.1818	2.1475	0.0000	1.0146
-3.5818	2.2058	-3.2091	2.0423	0.0000	0.8394
-3.6182	2.1124	-3.2364	1.9256	0.0091	0.5358
-3.6534	2.0190	-3.2636	1.8204	0.0091	0.2905
-3.6909	1.9372	-3.3091	1.6686	0.0091	0.0920

z	x, MHP	z	x, THP	z	x, BHP
-3.7273	1.8321	-3.3455	1.5051	0.0091	-0.0949
-3.7727	1.7270	-3.3636	1.4117	0.0273	-0.3284
-3.8000	1.6219	-3.4000	1.2832	0.0273	-0.5971
-3.8273	1.4934	-3.4273	1.1664	0.0091	-0.9007
-3.8546	1.3533	-3.4455	1.0029	0.0000	-1.1343
-3.8909	1.2365	-3.4636	0.8978	0.0000	-1.4613
-3.9091	1.1548	-3.4818	0.7577	-0.0091	-1.6481
-3.9364	1.0380	-3.4818	0.6175	-0.0091	-1.8233
-3.9546	0.9329	-3.4909	0.5008	-0.0091	-2.0102
-3.9727	0.8278	-3.4909	0.3372	-0.0091	-2.3138
-3.9818	0.7577	-3.5000	0.1154	-0.0091	-2.5941
-3.9818	0.6526	-3.4909	0.0102	-0.0182	-2.7810
-3.9909	0.5708	-3.4818	-0.0949	-0.0182	-2.9795
-3.9909	0.4774	-3.4818	-0.2233		
-4.0000	0.3723	-3.4818	-0.3518		
-4.0068	0.2905	-3.4636	-0.4336		
-4.0079	0.1854	-3.4546	-0.5503		
-4.0068	0.0920	-3.4364	-0.6554		
-4.0000	-0.0248	-3.4364	-0.7255		
-3.9898	-0.1386	-3.4182	-0.8073		
-3.9818	-0.2350	-3.4091	-0.9124		
-3.9727	-0.3168	-3.3818	-1.0525		
-3.9716	-0.3985	-3.3546	-1.1226		
-3.9636	-0.5036	-3.3273	-1.2394		
-3.9455	-0.6087	-3.2909	-1.3912		
-3.9364	-0.6788	-3.2546	-1.5197		
-3.9182	-0.7606	-3.2091	-1.6598		
-3.9000	-0.8540	-3.1727	-1.7883		
-3.8818	-0.9708	-3.1455	-1.9168		
-3.8557	-1.0759	-3.1000	-2.0335		
-3.8364	-1.1693	-3.0727	-2.1153		
-3.8091	-1.2627	-3.0455	-2.2204		
-3.7909	-1.3562	-3.0091	-2.3605		
-3.7625	-1.4598	-2.9546	-2.4890		
-3.7273	-1.5430	-2.9364	-2.5474		
-3.7000	-1.6248	-2.9091	-2.6408		
-3.6784	-1.6832	-2.8727	-2.7576		
-3.6329	-1.8000	-2.8273	-2.8627		
-3.5807	-1.9371	-2.7818	-2.9912		
-3.5534	-2.0321				
-3.5068	-2.1153				
-3.4772	-2.1854				
-3.4273	-2.2788				

z	x, MHP	z	x, THP	z	x, BHP
-3.3818	-2.3722				
-3.3238	-2.4860				
-3.3204	-2.5124				
-3.2931	-2.5474				
-3.2659	-2.6058				
-3.1693	-2.7621				
-3.1160	-2.8468				
-3.0444	-2.9576				

Table C.4(a). Interface shapes for SCN-ACE alloy, no growth, vertical planes.

z	y, MVP	z	y, FVP
-3.4868	2.9414	-2.4176	2.9180
-3.5111	2.8477	-2.4176	2.7539
-3.5354	2.7305	-2.4176	2.6016
-3.5597	2.6484	-2.4054	2.4609
-3.5719	2.5430	-2.3933	2.2969
-3.5840	2.4375	-2.3690	2.1094
-3.5962	2.3438	-2.3446	1.8984
-3.6205	2.2500	-2.3325	1.7578
-3.6205	2.1328	-2.2960	1.5938
-3.6326	2.0273	-2.2596	1.4531
-3.6448	1.9219	-2.2110	1.2891
-3.6569	1.7930	-2.1502	1.1133
-3.6691	1.6641	-2.0652	0.9492
-3.6691	1.5703	-2.0044	0.8086
-3.6569	1.4414	-1.9437	0.6680
-3.6326	1.3477	-1.8708	0.5273
-3.6083	1.2305	-1.7614	0.3633
-3.5719	1.1016	-1.6521	0.1992
-3.5597	1.0430	-1.5548	0.0703
-3.5354	0.9375	-1.4576	-0.0469
-3.4990	0.8320	-1.3483	-0.1875
-3.4382	0.7383	-1.2389	-0.3164
-3.4139	0.6680	-1.1174	-0.4453
-3.3532	0.5625	-0.9959	-0.5859
-3.2924	0.4453	-0.8501	-0.7266
-3.1831	0.3047	-0.7407	-0.8555
-3.0858	0.1875	-0.6435	-0.9727
-3.0008	0.0703	-0.5342	-1.0898
-2.9279	-0.0352	-0.4127	-1.2305
-2.8307	-0.1406	-0.3155	-1.3477
-2.7335	-0.2344	-0.2304	-1.4414

z	y, MVP	z	y, FVP
-2.6484	-0.3398	-0.1454	-1.5586
-2.5634	-0.4219	-0.0360	-1.6758
-2.4783	-0.4922	0.0734	-1.8164
-2.3811	-0.5859	0.1706	-1.9570
-2.2717	-0.6914	0.2799	-2.0859
-2.1259	-0.7969	0.3771	-2.2383
-1.9558	-0.9141	0.5108	-2.3672
-1.8100	-1.0195	0.6201	-2.5313
-1.6764	-1.1016	0.7660	-2.6836
-1.5670	-1.1719	0.8996	-2.8477
-1.4698	-1.2422	1.0333	-3.0000
-1.3483	-1.3242		
-1.2025	-1.4297		
-1.0931	-1.5000		
-0.9473	-1.6055		
-0.8258	-1.6875		
-0.6921	-1.7813		
-0.5463	-1.8867		
-0.4127	-1.9688		
-0.2790	-2.0625		
-0.1575	-2.1680		
-0.0481	-2.2500		
0.0977	-2.3672		
0.2556	-2.4961		
0.4014	-2.6016		
0.5715	-2.6953		
0.7174	-2.8125		
0.8510	-2.8945		
1.0090	-3.0000		

Table C.4(b). Interface shapes for SCN-ACE alloy, no growth, horizontal plane

z	x, MHP
-2.2757	2.9888
-2.3437	2.9214
-2.4118	2.8541
-2.4685	2.8092
-2.5479	2.7194
-2.6387	2.6408
-2.7067	2.5510
-2.7861	2.4500
-2.8882	2.3377
-2.9563	2.2142

z	x, MHP
-3.0130	2.1356
-3.1037	2.0122
-3.1831	1.8887
-3.2285	1.7989
-3.2966	1.6642
-3.3420	1.5744
-3.3873	1.4621
-3.4440	1.3499
-3.5008	1.2264
-3.5348	1.1029
-3.5915	0.9570
-3.6142	0.8110
-3.6369	0.6202
-3.6709	0.4743
-3.6823	0.3059
-3.6823	0.1712
-3.6823	0.0140
-3.6823	-0.1207
-3.6709	-0.2554
-3.6709	-0.4462
-3.6482	-0.6146
-3.6369	-0.7718
-3.5915	-0.9626
-3.5688	-1.1422
-3.5008	-1.3330
-3.4440	-1.5126
-3.3420	-1.7147
-3.2285	-1.8718
-3.1378	-2.0178
-3.0357	-2.1974
-2.9449	-2.2984
-2.8201	-2.4556
-2.7748	-2.5341
-2.6727	-2.6352
-2.5366	-2.7699
-2.3891	-2.8821
-2.2303	-2.9944

Table C.5(a) Interface shapes for alloy SCN-ACE, 2 μm/s growth, vertical planes.

z	y, MVP	z	y, FVP
-4.0167	2.9764	-3.2597	2.9764
-4.0425	2.8937	-3.2425	2.8465
-4.0597	2.7992	-3.2425	2.7402
-4.0683	2.7047	-3.2339	2.5984
-4.0855	2.5984	-3.2167	2.4567
-4.0941	2.4685	-3.2081	2.2913
-4.1113	2.3622	-3.1736	2.1614
-4.1199	2.2441	-3.1306	1.9724
-4.1285	2.1378	-3.0876	1.8307
-4.1371	2.0079	-3.0446	1.6772
-4.1371	1.8543	-2.9844	1.5118
-4.1457	1.7008	-2.9242	1.3346
-4.1457	1.5591	-2.8812	1.1693
-4.1371	1.4291	-2.8210	1.0276
-4.1199	1.2874	-2.7521	0.8268
-4.0941	1.1693	-2.6747	0.6614
-4.0683	1.0512	-2.6145	0.5315
-4.0253	0.8858	-2.5543	0.4134
-3.9651	0.7559	-2.4683	0.2598
-3.9048	0.6142	-2.3908	0.1417
-3.8446	0.4961	-2.2876	0.0000
-3.7758	0.3661	-2.2016	-0.1535
-3.7156	0.2480	-2.1070	-0.2598
-3.6382	0.1417	-1.9951	-0.4016
-3.5780	0.0354	-1.9005	-0.5197
-3.4833	-0.0827	-1.7887	-0.6378
-3.3973	-0.2008	-1.6596	-0.7913
-3.2941	-0.2953	-1.5392	-0.9331
-3.1650	-0.4252	-1.4274	-1.0630
-3.0790	-0.5079	-1.3069	-1.2165
-2.9586	-0.6142	-1.1607	-1.4173
-2.8554	-0.7205	-1.0059	-1.5709
-2.7349	-0.8150	-0.8940	-1.7126
-2.6231	-0.9213	-0.7392	-1.8661
-2.5113	-0.9921	-0.6360	-1.9724
-2.3994	-1.0866	-0.5155	-2.1260
-2.2704	-1.1811	-0.3865	-2.2795
-2.1156	-1.2992	-0.2919	-2.3858
-2.0037	-1.3819	-0.2059	-2.5158
-1.9005	-1.4528	-0.1112	-2.6221
-1.7887	-1.5354	-0.0252	-2.7165

z	y, MVP	z	y, FVP
-1.6854	-1.6063	0.0780	-2.8819
-1.5564	-1.7008	0.1641	-3.0000
-1.4446	-1.7835		
-1.3328	-1.8661		
-1.2553	-1.9252		
-1.1693	-1.9961		
-1.0919	-2.0433		
-1.0145	-2.1024		
-0.9284	-2.1732		
-0.8424	-2.2441		
-0.7478	-2.3268		
-0.6360	-2.4095		
-0.5327	-2.5039		
-0.4381	-2.5748		
-0.3521	-2.6457		
-0.2575	-2.7047		
-0.1456	-2.7992		
-0.0510	-2.8701		
0.0608	-2.9409		
0.1296	-3.0000		

Table C.5(b) Interface shapes for alloy SCN-ACE, 2 μm/s growth, horizontal planes.

z	x, MHP	z	x, THP	z	x, BHP
-3.3458	3.0000	-3.2020	3.0000	0.0958	2.8828
-3.4016	2.8828	-3.2340	2.9063	0.0958	2.7539
-3.4575	2.8125	-3.2739	2.7773	0.0878	2.6367
-3.5134	2.6953	-3.2978	2.6484	0.0799	2.4844
-3.5853	2.5664	-3.3298	2.5313	0.0799	2.2969
-3.6332	2.4492	-3.3777	2.3789	0.0719	2.1094
-3.7051	2.3086	-3.4176	2.2500	0.0639	1.9102
-3.7530	2.1914	-3.4655	2.1094	0.0639	1.7344
-3.8009	2.0625	-3.5055	1.9805	0.0479	1.5469
-3.8488	1.9102	-3.5534	1.8398	0.0399	1.3477
-3.8967	1.7813	-3.6093	1.6641	0.0240	1.1602
-3.9446	1.5938	-3.6492	1.5117	0.0080	0.9492
-3.9925	1.4297	-3.6891	1.3359	0.0000	0.7500
-4.0325	1.2539	-3.7210	1.1602	-0.0080	0.4805
-4.0564	1.1016	-3.7530	1.0078	-0.0160	0.2695
-4.0884	0.9492	-3.7690	0.8789	-0.0160	0.0586
-4.1043	0.7734	-3.7929	0.6914	-0.0160	-0.1992
-4.1203	0.5977	-3.8089	0.5391	-0.0160	-0.3633
-4.1283	0.4102	-3.8249	0.3398	-0.0160	-0.5391

z	x, MHP	z	x, THP	z	x, BHP
-4.1283	0.2109	-3.8328	0.1641	-0.0160	-0.6797
-4.1283	0.0234	-3.8328	0.0234	-0.0160	-0.9393
-4.1283	-0.1523	-3.8249	-0.1641	-0.0160	-1.2422
-4.1123	-0.3164	-3.8169	-0.3281	-0.0080	-1.4766
-4.1043	-0.5273	-3.8089	-0.4922	0.0000	-1.6992
-4.0884	-0.6914	-3.7929	-0.7031	0.0080	-1.9688
-4.0804	-0.8438	-3.7849	-0.8438	0.0160	-2.1445
-4.0484	-1.0078	-3.7530	-1.0313	0.0160	-2.3203
-4.0245	-1.1836	-3.7290	-1.1602	0.0160	-2.5195
-3.9846	-1.3594	-3.7051	-1.3125	0.0160	-2.7070
-3.9526	-1.5117	-3.6572	-1.5234	0.0160	-2.8594
-3.9207	-1.6641	-3.6172	-1.6641	0.0160	-2.9648
-3.8887	-1.7930	-3.5853	-1.8164		
-3.8648	-1.9219	-3.5534	-1.9688		
-3.8249	-2.0508	-3.5055	-2.1328		
-3.7929	-2.1680	-3.4655	-2.2852		
-3.7450	-2.2734	-3.4256	-2.4492		
-3.7051	-2.3789	-3.3857	-2.5781		
-3.6731	-2.4844	-3.3378	-2.7539		
-3.6252	-2.5781	-3.2739	-2.9180		
-3.5773	-2.6836				
-3.5214	-2.8008				
-3.4655	-2.8945				
-3.4096	-2.9883				

APPENDIX D - AVERAGED INTERFACE SHAPES IN X-Z PLANES

The interface is assumed to be symmetric about x. Since the raw data for these interface locations contained slight asymmetry, a set of results which are averaged to make them symmetric are also provided. It is intended that these averaged results be used for validating numerical simulations. Both the raw and averaged data is plotted in the figures. All values shown are in mm.

The raw data was obtained by manually plotting points along the interface images using computer software. Since there was no systematic control over the x-location of each data point, the data points obtained were not at regular spacings on each side of the $x = 0$ axis (i.e. data points were obtained at $x = +0.13, +0.22, +0.36$ etc. and $x = -0.11, -0.23, -0.33$ etc. rather than at $x = \pm 0.1, \pm 0.2$ ± 0.3 etc.). This makes averaging the results in each half-plane cumbersome. The following procedure was used. Results for the $x > 0$ half-plane were interpolated to points corresponding to x locations for the $x < 0$ half-plane (i.e. interpolated results found at $x = +0.11, +0.23, +0.33$ etc.). The same procedure was applied to the results in the $x < 0$ half plane (i.e. interpolated values found at $x = -0.13, -0.22, -0.36$ etc.). The sets of data (both raw and interpolated values) for each half-plane were then combined and averaged.

Since the front is assumed to be flat (no variation in z across the ampoule width) in the BHP, an arithmetic mean was used to determine the average z position rather than the procedure described above. The procedure detailed above produces a symmetric, but not necessarily flat, result.

Table D.1. Averaged values for pure SCN, no-growth case, horizontal planes.

z, avg.	x, MHP	z, avg.	x, THP	z, avg.	x, BHP
-0.9493	3.0000	-0.7958	3.0000	2.0610	3.0000
-0.9972	2.9641	-0.8212	2.9162	2.0610	2.8443
-1.0516	2.9162	-0.8432	2.8683	2.0610	2.8323
-1.0516	2.9162	-0.8527	2.8443	2.0610	2.7246
-1.1060	2.8683	-0.9067	2.7605	2.0610	2.6407
-1.1460	2.8323	-0.9228	2.7246	2.0610	2.6287
-1.1710	2.8084	-0.9578	2.6527	2.0610	2.5090
-1.1994	2.7725	-0.9967	2.5808	2.0610	2.4252
-1.2250	2.7365	-1.0125	2.5449	2.0610	2.4132
-1.2506	2.7006	-1.0587	2.4132	2.0610	2.2575
-1.2746	2.6647	-1.0687	2.3892	2.0610	2.1856
-1.3241	2.5995	-1.1066	2.2934	2.0610	2.1257
-1.3384	2.5808	-1.1331	2.2096	2.0610	2.0180
-1.3832	2.5090	-1.1507	2.1497	2.0610	1.9341
-1.4012	2.4731	-1.1913	2.0180	2.0610	1.8743
-1.4467	2.3772	-1.2108	1.9581	2.0610	1.7545
-1.4533	2.3653	-1.2297	1.8982	2.0610	1.7186
-1.5109	2.2695	-1.2707	1.7784	2.0610	1.5629
-1.5221	2.2455	-1.2741	1.7665	2.0610	1.5509
-1.5702	2.1377	-1.3058	1.6347	2.0610	1.3952

z, avg.	x, MHP	z, avg.	x, THP	z, avg.	x, BHP
-1.5790	2.1138	-1.3103	1.6108	2.0610	1.3832
-1.6291	1.9820	-1.3367	1.4910	2.0610	1.2275
-1.6340	1.9701	-1.3497	1.4431	2.0610	1.2036
-1.6749	1.8862	-1.3806	1.3234	2.0610	1.1198
-1.6894	1.8503	-1.3934	1.2515	2.0610	1.0000
-1.7198	1.7665	-1.4108	1.1317	2.0610	0.9880
-1.7368	1.7186	-1.4234	1.0479	2.0610	0.8683
-1.7736	1.6108	-1.4390	0.9521	2.0610	0.7964
-1.7868	1.5749	-1.4491	0.8802	2.0610	0.7246
-1.8142	1.5030	-1.4609	0.7964	2.0610	0.5928
-1.8456	1.4072	-1.4723	0.7126	2.0610	0.5928
-1.8492	1.3952	-1.4841	0.6287	2.0610	0.3772
-1.8855	1.2635	-1.4918	0.5569	2.0610	0.3413
-1.8889	1.2515	-1.4950	0.4611	2.0610	0.2216
-1.9161	1.1437	-1.4983	0.4132	2.0610	0.1377
-1.9283	1.0958	-1.5104	0.2934	2.0610	0.0419
-1.9559	0.9880	-1.5121	0.2455		
-1.9649	0.9401	-1.5121	0.0778		
-1.9790	0.8443	-1.5121	0.0539		
-1.9896	0.7725				
-1.9977	0.7006				
-2.0047	0.6048				
-2.0109	0.5569				
-2.0283	0.4252				
-2.0298	0.4132				
-2.0350	0.2814				
-2.0366	0.2335				
-2.0407	0.1018				
-2.0426	0.0419				

Table D.2. Averaged values for pure SCN, growth at 40 μm/s, horizontal planes.

z, avg.	x, MHP
-4.4080	3.0000
-4.5080	2.9408
-4.5619	2.9090
-4.5917	2.8886
-4.6737	2.8364
-4.7112	2.8233
-4.7448	2.8045
-4.8051	2.7711
-4.9032	2.7058
-4.9579	2.6927
-4.9666	2.6870

z, avg.	x, MHP
-5.0714	2.6144
-5.1174	2.5825
-5.1866	2.5361
-5.2975	2.4577
-5.3046	2.4520
-5.4080	2.3663
-5.4294	2.3475
-5.5315	2.2618
-5.5564	2.2431
-5.6695	2.1443
-5.7040	2.1125
-5.8131	2.0137
-5.8190	2.0080
-5.9253	1.8962
-5.9701	1.8513
-6.0526	1.7787
-6.1078	1.7207
-6.1708	1.6481
-6.2323	1.5902
-6.2776	1.5437
-6.3464	1.4596
-6.3720	1.4262
-6.4250	1.3609
-6.4294	1.3551
-6.5214	1.2303
-6.5251	1.2246
-6.6283	1.0867
-6.6330	1.0809
-6.6954	0.9822
-6.7226	0.9242
-6.7503	0.8777
-6.7827	0.8198
-6.8200	0.7210
-6.8335	0.6761
-6.8779	0.5194
-6.9034	0.4468
-6.9086	0.4280
-6.9340	0.2640
-6.9345	0.2452
-6.9372	0.1465
-6.9420	0.0624

Table D.3. Averaged values for pure SCN, growth at 2 μm/s, horizontal planes.

z, avg.	x, MHP	z, avg.	x, THP	z, avg.	x, BHP
-3.0449	3.0000	-2.8114	2.9912	-0.0047	2.9795
-3.0750	2.9576	-2.8534	2.8949	-0.0047	2.9533
-3.1197	2.8949	-2.8695	2.8627	-0.0047	2.8015
-3.1519	2.8468	-2.8900	2.8248	-0.0047	2.7810
-3.1896	2.7898	-2.9092	2.7781	-0.0047	2.6029
-3.2064	2.7621	-2.9193	2.7576	-0.0047	2.5941
-3.2178	2.7431	-2.9459	2.6964	-0.0047	2.3138
-3.2912	2.6380	-2.9681	2.6408	-0.0047	2.3110
-3.3157	2.6058	-2.9828	2.6029	-0.0047	2.1124
-3.3418	2.5679	-3.0017	2.5474	-0.0047	2.0102
-3.3516	2.5474	-3.0222	2.4890	-0.0047	1.9139
-3.3737	2.5124	-3.0233	2.4861	-0.0047	1.8233
-3.3818	2.4860	-3.0568	2.3927	-0.0047	1.6803
-3.3876	2.4745	-3.0674	2.3605	-0.0047	1.6481
-3.4311	2.3927	-3.0883	2.2759	-0.0047	1.5168
-3.4414	2.3722	-3.1033	2.2204	-0.0047	1.4613
-3.4768	2.2993	-3.1231	2.1475	-0.0047	1.2482
-3.4868	2.2788	-3.1315	2.1153	-0.0047	1.1343
-3.5240	2.2058	-3.1531	2.0423	-0.0047	1.0146
-3.5335	2.1854	-3.1556	2.0335	-0.0047	0.9007
-3.5619	2.1153	-3.1892	1.9256	-0.0047	0.8394
-3.5633	2.1124	-3.1921	1.9167	-0.0047	0.5971
-3.6009	2.0320	-3.2148	1.8204	-0.0047	0.5358
-3.6053	2.0190	-3.2230	1.7883	-0.0047	0.3284
-3.6358	1.9372	-3.2578	1.6686	-0.0047	0.2905
-3.6358	1.9371	-3.2601	1.6598	-0.0047	0.0949
-3.6740	1.8321	-3.2984	1.5197	-0.0047	0.0920
-3.6870	1.8000	-3.3021	1.5051		
-3.7170	1.7270	-3.3244	1.4117		
-3.7312	1.6832	-3.3302	1.3912		
-3.7496	1.6248	-3.3584	1.2832		
-3.7505	1.6219	-3.3688	1.2394		
-3.7720	1.5430	-3.3858	1.1664		
-3.7878	1.4934	-3.3934	1.1226		
-3.7982	1.4598	-3.4109	1.0525		
-3.8225	1.3562	-3.4185	1.0029		
-3.8230	1.3533	-3.4351	0.9124		
-3.8459	1.2627	-3.4370	0.8978		
-3.8538	1.2365	-3.4468	0.8073		
-3.8711	1.1693	-3.4555	0.7577		
-3.8742	1.1548	-3.4591	0.7255		

z, avg.	x, MHP	z, avg.	x, THP	z, avg.	x, BHP
-3.8916	1.0759	-3.4591	0.6554		
-3.9007	1.0380	-3.4624	0.6175		
-3.9149	0.9708	-3.4708	0.5503		
-3.9211	0.9329	-3.4747	0.5008		
-3.9341	0.8540	-3.4773	0.4335		
-3.9389	0.8278	-3.4864	0.3518		
-3.9498	0.7606	-3.4864	0.3372		
-3.9503	0.7577	-3.4887	0.2233		
-3.9591	0.6788	-3.4909	0.1154		
-3.9608	0.6526	-3.4900	0.0949		
-3.9661	0.6087	-3.4909	0.0102		
-3.9715	0.5708				
-3.9773	0.5036				
-3.9783	0.4774				
-3.9847	0.3985				
-3.9860	0.3723				
-3.9887	0.3168				
-3.9912	0.2905				
-3.9946	0.2350				
-3.9969	0.1854				
-3.9986	0.1386				
-4.0004	0.0920				
-4.0000	0.0248				

Table D.4. Averaged values for SCN-ACE alloy, no-growth case, horizontal planes.

z, avg.	x, MHP
-2.2303	2.9944
-2.2569	2.9888
-2.3386	2.9214
-2.3863	2.8821
-2.4189	2.8541
-2.4767	2.8092
-2.5199	2.7699
-2.5678	2.7194
-2.6528	2.6408
-2.6578	2.6352
-2.7322	2.5510
-2.7474	2.5341
-2.8009	2.4556
-2.8054	2.4500
-2.9010	2.3377
-2.9274	2.2984

z, avg.	x, MHP
-2.9884	2.2142
-3.0021	2.1974
-3.0419	2.1356
-3.1187	2.0178
-3.1225	2.0122
-3.2006	1.8887
-3.2101	1.8718
-3.2549	1.7989
-3.3065	1.7147
-3.3320	1.6642
-3.3774	1.5744
-3.4055	1.5126
-3.4237	1.4621
-3.4697	1.3499
-3.4763	1.3330
-3.5198	1.2264
-3.5464	1.1422
-3.5543	1.1029
-3.5904	0.9626
-3.5922	0.9570
-3.6209	0.8110
-3.6279	0.7717
-3.6424	0.6202
-3.6432	0.6146
-3.6690	0.4743
-3.6719	0.4462
-3.6766	0.3059
-3.6766	0.2554
-3.6801	0.1712
-3.6823	0.1207
-3.6823	0.0140

Table D.5. Averaged values for SCN-ACE alloy, growth at 2 μm/s, horizontal planes.

z, avg.	x, MHP	z, avg.	x, THP	z, avg.	x, BHP
-3.3742	3.0000	-3.2220	3.0000	0.0232	2.9648
-3.3805	2.9883	-3.2519	2.9180	0.0232	2.8828
-3.4308	2.8945	-3.2562	2.9063	0.0232	2.8594
-3.4371	2.8828	-3.3013	2.7773	0.0232	2.7539
-3.4860	2.8125	-3.3080	2.7539	0.0232	2.7070
-3.4923	2.8008	-3.3322	2.6484	0.0232	2.6367
-3.5426	2.6953	-3.3513	2.5781	0.0232	2.5195
-3.5486	2.6836	-3.3650	2.5313	0.0232	2.4844

z, avg.	x, MHP	z, avg.	x, THP	z, avg.	x, BHP
-3.6020	2.5781	-3.3906	2.4492	0.0232	2.3203
-3.6083	2.5664	-3.4102	2.3789	0.0232	2.2969
-3.6460	2.4844	-3.4361	2.2852	0.0232	2.1445
-3.6585	2.4492	-3.4462	2.2500	0.0232	2.1094
-3.6871	2.3789	-3.4815	2.1328	0.0232	1.9688
-3.7184	2.3086	-3.4889	2.1094	0.0232	1.9102
-3.7322	2.2734	-3.5277	1.9805	0.0232	1.7344
-3.7676	2.1914	-3.5314	1.9688	0.0232	1.6992
-3.7773	2.1680	-3.5669	1.8398	0.0232	1.5469
-3.8113	2.0625	-3.5731	1.8164	0.0232	1.4766
-3.8147	2.0508	-3.6133	1.6641	0.0232	1.3477
-3.8550	1.9219	-3.6133	1.6641	0.0232	1.2422
-3.8579	1.9102	-3.6516	1.5234	0.0232	1.1602
-3.8906	1.7930	-3.6545	1.5117	0.0232	0.9492
-3.8942	1.7813	-3.6944	1.3359	0.0232	0.9393
-3.9237	1.6641	-3.6992	1.3125	0.0232	0.7500
-3.9400	1.5938	-3.7250	1.1602	0.0232	0.6797
-3.9606	1.5117	-3.7250	1.1602	0.0232	0.5391
-3.9812	1.4297	-3.7505	1.0313	0.0232	0.4805
-3.9965	1.3594	-3.7550	1.0078	0.0232	0.3633
-4.0205	1.2539	-3.7740	0.8789	0.0232	0.2695
-4.0340	1.1836	-3.7792	0.8438	0.0232	0.1992
-4.0460	1.1016	-3.7922	0.7031	0.0232	0.0586
-4.0623	1.0078	-3.7934	0.6914		
-4.0741	0.9492	-3.8071	0.5391		
-4.0892	0.8438	-3.8108	0.4922		
-4.0942	0.7734	-3.8206	0.3398		
-4.1001	0.6914	-3.8211	0.3281		
-4.1089	0.5977	-3.8288	0.1641		
-4.1138	0.5273	-3.8288	0.1641		
-4.1185	0.4102	-3.8328	0.0234		
-4.1203	0.3164				
-4.1254	0.2109				
-4.1283	0.1523				
-4.1283	0.0234				

APPENDIX E - Stereoscopic Imaging Velocimetry (SIV)

An attempt to obtain measurements of the convective velocity field with Stereoscopic Imaging Velocimetry (SIV) was part of this experiment. Ultimately, this was not successful; an outline of the equipment and procedure for obtaining velocity measurements via SIV is given here, as is a brief discussion of possible reasons why no good data was able to be obtained. Two high-definition CCD video cameras, with zoom lenses, are mounted in the vertical and horizontal planes and are focused on the center of the sample between the two copper jackets. Each of these cameras feed to a digital videotape recorder (temporary data storage), digital laser disc recorder (permanent high-fidelity data storage) and monitor (viewing). Under special polarized lighting conditions, the motion of the seed particles in the melt can be resolved by the cameras and recorded onto digital laser disc. The 90° separated views provided by the two cameras enable the positions (and hence, velocities) of the particles to be tracked in three dimensions. The images are analyzed via a digital computer which uses sophisticated image processing and tracking techniques in order to determine the positions and velocities of a large number of particles. These results are then averaged to obtain the final set of velocities. A sample frame taken from the images used for SIV analysis is shown in figure 3.

Calibration for SIV consists of viewing a high-contrast image of an array of dots which is of the same size as the desired volume in which measurements are to take place. The dots are spaced at a known distance apart (1 mm for this experiment). This calibration enables the image processing software to reconcile the size of the particles and the movement of the particles to a reference distance and coordinate system. For this experiment, calibration was achieved by the use of an empty ampoule containing the calibration image which was then mounted in the furnace and viewed by the cameras. The ampoule containing the calibration image is different from that used to take the measurements, however, the calibration technique considers only the calibration image. Therefore, using a different ampoule is not anticipated to be a source of experimental error.

A more detailed description of SIV techniques is available in [19].

Possible reasons why no good data was obtained from SIV are outlined below.

- The seed particles in the ampoule varied in size, making it difficult for the computer algorithms to sort the location of the particles. The smaller particles in the sample may appear to be further away from the camera than larger particles where in actuality they are in the same plane.
- The number density of particles was too high; while this aids flow visualization it detracts from SIV measurements by overwhelming the particle-tracking algorithms with many particle traces.
- The ampoule contained many defects that produced "bright spots" in the SIV images. Particle traces that pass into these spots are often lost.
- The ampoule was not perfectly square on the outside, leading to distortion in the filmed motion of the particles.
- Errors were made and could not be found and corrected in the calibration and/or definition of a consistent coordinate system and/or SIV software

A possible solution to these difficulties is to use uniform seed particles in an ampoule with a square, polished silica or glass cross-section and analyze new images using this ampoule. This should eliminate most of the problems identified above and furnish an acceptable yield of velocity measurements.

APPENDIX F - Velocity Measurements

This appendix contains raw and processed data for particle positions and velocities. The procedure used to process the data is outlined in the pure SCN results section (section 3).

Table F.1. Raw data for Particle #8 locations.

x-z data set

x (mm)	z_x (mm)	t_x (sec)
0.788	2.020	0.000
0.848	1.515	0.433
0.924	0.909	0.967
1.030	0.330	1.500
1.150	-0.220	2.033
1.300	-0.697	2.633
1.400	-1.120	3.703
1.380	-1.120	3.803
1.210	-0.800	4.503
1.090	-0.330	5.037
0.960	0.230	5.570
0.820	1.091	6.370
0.788	1.667	6.900

y-z data set

y (mm)	z_y (mm)	t_y (sec)
1.390	2.280	0.067
1.480	1.750	0.500
1.590	1.140	1.033
1.714	0.500	1.567
1.840	-0.110	2.100
1.864	-0.607	2.700
1.375	-1.020	3.500
1.000	-0.982	3.933
0.375	-0.661	4.500
-0.140	-0.180	5.033
-0.571	0.430	5.600
-0.946	1.230	6.300
-1.110	1.853	6.833

Table F.2. Raw data for Particle #12 locations.

x-z data set

x (mm)	z_x (mm)	t_x (sec)
0.325	2.430	0.000
0.330	2.095	0.300
0.370	1.390	0.833
0.398	0.690	1.367
0.477	0.000	1.900
0.560	-0.650	2.433
0.634	-1.230	2.967
0.690	-1.710	3.767
0.660	-1.660	4.233
0.580	-1.300	4.800
0.504	-0.554	5.500
0.424	0.250	6.133
0.360	1.260	6.933
0.290	2.215	7.733

y-z data set

y (mm)	z_y (mm)	t_y (sec)
1.520	2.460	0.100
1.640	1.480	0.800
1.860	0.345	1.667
2.010	-0.340	2.200
2.136	-0.955	2.733
2.040	-1.330	3.167
1.740	-1.600	3.600
1.244	-1.620	4.033
0.603	-1.380	4.566
-0.060	-0.800	5.166
-0.540	-0.174	5.700
-1.000	0.686	6.400
-1.237	1.376	6.933
-1.450	2.350	7.733

Table F.3. Raw data for Particle #13 locations.

x-z data set

x (mm)	z_x (mm)	t_x (sec)
0.040	2.310	0.000
0.056	1.747	0.433
0.056	1.193	0.833
0.056	0.611	1.267
0.070	-0.056	1.767
0.084	-0.611	2.200
0.078	-1.165	2.700
0.092	-1.560	3.133
0.081	-1.807	3.667
0.092	-1.740	4.100
0.070	-1.454	4.600
0.060	-1.000	5.060
0.056	-0.168	5.760
0.056	0.500	6.293
0.064	1.176	6.826
0.056	2.145	7.626

y-z data set

y (mm)	z_y (mm)	t_y (sec)
1.530	2.246	0.133
1.590	1.895	0.400
1.714	1.246	0.866
1.850	0.630	1.333
2.025	-0.058	1.866
2.156	-0.598	2.300
2.190	-1.047	2.733
2.087	-1.286	3.000
1.910	-1.467	3.266
1.600	-1.590	3.533
1.250	-1.610	3.866
0.696	-1.395	4.333
-0.109	-0.797	5.033
-0.616	-0.178	5.566
-1.018	0.457	6.099
-1.304	1.105	6.633
-1.514	1.775	7.166
-1.640	2.406	7.699

Table F.4. Processed data for Particle #8 locations.

x-z data set

x (mm)	z_x + 0.1 (mm)	t_x (sec)
0.788	2.120	0.000
0.848	1.615	0.433
0.924	1.009	0.967
1.030	0.430	1.500
1.150	-0.120	2.033
1.300	-0.597	2.633
1.400	-1.020	3.703
1.380	-1.020	3.803
1.210	-0.700	4.503
1.090	-0.230	5.037
0.960	0.330	5.570
0.820	1.191	6.370
0.788	1.767	6.900

y-z data set

y (mm)	z_y - 0.1 (mm)	t_y - 1/30 (sec)
1.390	2.180	0.033
1.480	1.650	0.467
1.590	1.040	1.000
1.714	0.400	1.533
1.840	-0.210	2.067
1.864	-0.707	2.667
1.375	-1.120	3.467
1.000	-1.082	3.900
0.375	-0.761	4.466
-0.140	-0.280	5.000
-0.571	0.330	5.566
-0.946	1.130	6.266
-1.110	1.753	6.800

Table F.5. Processed data for Particle #12 locations.

x-z data set

x (mm)	z_x + 0.043 (mm)	t_x (sec)
0.325	2.473	0.000
0.330	2.138	0.300
0.370	1.433	0.833
0.398	0.733	1.367
0.477	0.043	1.900
0.560	-0.607	2.433
0.634	-1.187	2.967
0.690	-1.667	3.767
0.660	-1.617	4.233
0.580	-1.257	4.800
0.504	-0.511	5.500
0.424	0.293	6.133
0.360	1.303	6.933
0.290	2.258	7.733

y-z data set

y (mm)	z_y - 0.043 (mm)	t_y + 1/30 (sec)
1.520	2.417	0.133
1.640	1.437	0.833
1.860	0.302	1.700
2.010	-0.383	2.233
2.136	-0.998	2.767
2.040	-1.373	3.200
1.740	-1.643	3.633
1.244	-1.663	4.066
0.603	-1.423	4.600
-0.060	-0.843	5.200
-0.540	-0.217	5.733
-1.000	0.643	6.433
-1.237	1.333	6.966
-1.450	2.307	7.766

Table F.6. Processed data for Particle #13 locations.

x-z data set

x (mm)	z_x + 0.08 (mm)	t_x (sec)
0.040	2.390	0.000
0.056	1.827	0.433
0.056	1.273	0.833
0.056	0.691	1.267
0.070	0.024	1.767
0.084	-0.531	2.200
0.078	-1.085	2.700
0.092	-1.480	3.133
0.081	-1.727	3.667
0.092	-1.660	4.100
0.070	-1.374	4.600
0.060	-0.920	5.060
0.056	-0.088	5.760
0.056	0.580	6.293
0.064	1.256	6.826
0.056	2.225	7.626

y-z data set

y (mm)	z_y + 0.08 (mm)	t_y + 1/30 (sec)
1.530	2.166	0.167
1.590	1.815	0.433
1.714	1.166	0.900
1.850	0.550	1.366
2.025	-0.138	1.900
2.156	-0.678	2.333
2.190	-1.127	2.766
2.087	-1.366	3.033
1.910	-1.547	3.300
1.600	-1.670	3.566
1.250	-1.690	3.899
0.696	-1.475	4.366
-0.109	-0.877	5.066
-0.616	-0.258	5.599
-1.018	0.377	6.133
-1.304	1.025	6.666
-1.514	1.695	7.199
-1.640	2.326	7.733

Table F.7. Processed velocity data for Particle #8. Velocities are found using the processed position and time data listed in Table F.4. The error estimate for V_z is calculated from (V_z, measured - V_z, interpolated)/2. The average value in this error estimate was determined to be 0.03534 mm/s.

For this and following tables (F.8 and F.9), velocities were determined at the mid-point between two adjacent locations and times. These centered time and space locations for each velocity value are denoted with a "c" subscript. Thus t_c is the average of the greater and lesser times used in determining the velocity, while x_c is the average of the two x values used to calculate the velocity V_x, etc.

In these tables, data from both x-z and y-z data sets are brought together. As a result, approximately half of the x_c and y_c values are obtained through interpolation and at each t_c. Also, there is one measured V_z and one interpolated V_z (though only V_z avg., the average of these two V_z values is provided).

t_c (sec)	x_c (mm)	y_c (mm)	z_c (mm)	V_x (mm/s)	V_y (mm/s)	V_z (avg.) (mm/s)
0.2167	0.8180	1.4281	1.8675	0.1385		-1.1655
0.2500	0.8226	1.4350	1.9150	0.1388	0.2077	-1.1933
0.7000	0.8860	1.5281	1.3120	0.1425	0.2064	-1.1428
0.7333	0.8907	1.5350	1.3450	0.1460	0.2063	-1.1385
1.2333	0.9770	1.6443	0.7195	0.1988	0.2309	-1.1411
1.2666	0.9836	1.6520	0.7200	0.2004	0.2325	-1.1412
1.7666	1.0900	1.7691	0.1550	0.2250	0.2360	-1.0893
1.7999	1.0975	1.7770	0.0950	0.2265	0.2363	-1.0806
2.3332	1.2250	1.8507	-0.3585	0.2500	0.0515	-0.8209
2.3665	1.2333	1.8520	-0.4585	0.2438	0.0400	-0.8037
3.0665	1.3405	1.6195	-0.9135	0.1125	-0.6113	-0.4801
3.1682	1.3500	1.5574	-0.8085	0.0935	-0.6532	-0.4060
3.6832	1.4040	1.1875	-1.1010	-0.1649	-0.8655	0.0202
3.7532	1.3900	1.1269	-1.0200	-0.2000	-0.8987	0.0774
4.1532	1.2950	0.7205	-0.8600	-0.2429	-1.0888	0.4975
4.1831	1.2877	0.6875	-0.9215	-0.2420	-1.1031	0.5221
4.7331	1.1583	0.1175	-0.5205	-0.2261	-0.9657	0.8858
4.7699	1.1500	0.0820	-0.4650	-0.2250	-0.9520	0.8975
5.2830	1.0299	-0.3555	0.0250	-0.2431	-0.7607	1.0601
5.3032	1.0250	-0.3708	0.0500	-0.2438	-0.7535	1.0644
5.9163	0.8994	-0.7585	0.7300	-0.1805	-0.5357	1.1085
5.9698	0.8900	-0.7871	0.7605	-0.1750	-0.5159	1.1107
6.5330	0.8101	-1.0280	1.4415	-0.0779	-0.3075	1.1267
6.6348	0.8040	-1.0593	1.4790	-0.0604		1.0868
6.8998	0.7880		1.7670			

Table F.8. Processed velocity data for Particle #12. Velocities are found using the processed position and time data listed in Table F.5. The error estimate for V_z is calculated from (V_z, measured - V_z, interpolated)/2. The average value in this error estimate was determined to be 0.01695 mm/s.

t_c (sec)	x_c (mm)	y_c (mm)	z_c (mm)	V_x (mm/s)	V_y (mm/s)	V_z (avg.) (mm/s)
0.1500	0.3275	1.5229	2.3055	0.0167		-1.1167
0.4833	0.3438	1.5800	1.9270	0.0633	0.1714	-1.3405
0.5667	0.3500	1.5943	1.7855	0.0750	0.1802	-1.3562
1.1000	0.3840	1.7077	1.0830	0.0525	0.2363	-1.3207
1.2666	0.3928	1.7500	0.8695	0.0824	0.2539	-1.3082
1.6333	0.4375	1.8431	0.3880	0.1481	0.2682	-1.2952
1.9666	0.4874	1.9350	-0.0405	0.1528	0.2813	-1.2657
2.1666	0.5185	1.9912	-0.2820	0.1556	0.2644	-1.2270
2.4999	0.5693	2.0730	-0.6905	0.1451	0.2363	-1.1450
2.6999	0.5970	2.1202	-0.8970	0.1388	0.0468	-1.0609
2.9832	0.6352	2.0880	-1.1855	0.1095	-0.2216	-0.8729
3.3665	0.6620	1.9246	-1.4270	0.0700	-0.6381	-0.6255
3.4165	0.6655	1.8900	-1.5080	0.0594	-0.6924	-0.5837
3.8498	0.6846	1.4920	-1.6530	-0.0325	-1.1447	-0.0533
3.9998	0.6750	1.3203	-1.6420	-0.0643	-1.1625	0.1075
4.3331	0.6459	0.9235	-1.5430	-0.1139	-1.2020	0.4490
4.5164	0.6200	0.7032	-1.4370	-0.1412	-1.1706	0.6263
4.8997	0.5691	0.2715	-1.1330	-0.1214	-1.1050	0.9313
5.1497	0.5420	-0.0047	-0.8840	-0.1086	-1.0146	1.0619
5.4664	0.5076	-0.3000	-0.5300	-0.1170	-0.9001	1.1682
5.8164	0.4640	-0.5948	-0.1090	-0.1263	-0.7622	1.2372
6.0830	0.4303	-0.7700	0.2130	-0.1091	-0.6571	1.2477
6.5330	0.3920	-1.0444	0.7980	-0.0800	-0.5019	1.2693
6.6997	0.3787	-1.1185	0.9880	-0.0816	-0.4444	1.2710
7.3330	0.3250	-1.3346	1.7805	-0.0875	-0.2752	1.2075
7.3663	0.3221	-1.3435	1.8200		-0.2663	1.2175

Table F.9. Processed velocity data for Particle #13. Velocities are found using the processed position and time data listed in Table F.6. The error estimate for V_z is calculated from (V_z, measured - V_z, interpolated)/2. The average value in this error estimate was determined to be 0.01652 mm/s.

t_c (sec)	x_c (mm)	y_c (mm)	z_c (mm)	V_x (mm/s)	V_y (mm/s)	V_z (avg.) (mm/s)
0.2167	0.0480	1.5413	2.1085	0.0369		-1.2993
0.2999	0.0511	1.5600	1.9905	0.0295	0.2251	-1.3170
0.6333	0.0560	1.6432	1.5500	0.0000	0.2618	-1.3835
0.6665	0.0560	1.6520	1.4905	0.0000	0.2658	-1.3858
1.0500	0.0560	1.7578	0.9820	0.0000	0.2867	-1.3386
1.1331	0.0560	1.7820	0.8580	0.0050	0.2915	-1.3308
1.5166	0.0630	1.8993	0.3575	0.0280	0.3191	-1.3155
1.6331	0.0663	1.9375	0.2060	0.0291	0.3281	-1.3055
1.9833	0.0770	2.0503	-0.2535	0.0323	0.3091	-1.2691
2.1164	0.0813	2.0905	-0.4080	0.0197	0.3023	-1.2395
2.4499	0.0810	2.1652	-0.8080	-0.0120	0.0997	-1.0922
2.5497	0.0798	2.1730	-0.9025	-0.0023	0.0785	-1.0526
2.8996	0.0846	2.1385	-1.2465	0.0316	-0.3863	-0.9115
2.9166	0.0852	2.1320	-1.2825	0.0332	-0.3993	-0.8854
3.1662	0.0917	1.9985	-1.4565	0.0050	-0.6639	-0.6737
3.3999	0.0867	1.7933	-1.6035	-0.0214	-1.0843	-0.4658
3.4328	0.0860	1.7550	-1.6085	-0.0181	-1.1628	-0.4451
3.7328	0.0827	1.4250	-1.6800	0.0115	-1.0501	0.0010
3.8832	0.0867	1.2671	-1.6935	0.0263	-1.0980	0.1546
4.1327	0.0909	0.9730	-1.5825	-0.0117	-1.1873	0.4389
4.3498	0.0812	0.7152	-1.5170	-0.0448	-1.1732	0.5481
4.7160	0.0675	0.2935	-1.1760	-0.0272	-1.1500	0.9044
4.8298	0.0650	0.1626	-1.1470	-0.0217	-1.1102	0.9279
5.3327	0.0584	-0.3625	-0.5673	-0.0078	-0.9507	1.1652
5.4098	0.0580	-0.4358	-0.5040	-0.0057	-0.9189	1.1765
5.8660	0.0560	-0.8170	0.0595	-0.0015	-0.7538	1.2127
6.0265	0.0560	-0.9380	0.2460	0.0000	-0.6773	1.2247
6.3993	0.0576	-1.1610	0.7008	0.0105	-0.5363	1.2394
6.5598	0.0600	-1.2471	0.9180	0.0150	-0.4868	1.2484
6.9326	0.0629	-1.4090	1.3600	0.0010	-0.3938	1.2468
7.2264	0.0600	-1.5204	1.7405	-0.0100	-0.2893	1.2124
7.4659	0.0576	-1.5770			-0.2363	1.1832

REPORT DOCUMENTATION PAGE

Form Approved
OMB No. 0704-0188

1. AGENCY USE ONLY (Leave blank)	2. REPORT DATE	3. REPORT TYPE AND DATES COVERED
	September 2000	Technical Memorandum

4. TITLE AND SUBTITLE

Directional Solidification of Pure Succinonitrile and a Succinonitrile-Acetone Alloy

5. FUNDING NUMBERS

WU-101-13-0A-00
NCC3-476

6. AUTHOR(S)

James E. Simpson, Henry C. de Groh, III, and Suresh V. Garimella

7. PERFORMING ORGANIZATION NAME(S) AND ADDRESS(ES)

National Aeronautics and Space Administration
John H. Glenn Research Center at Lewis Field
Cleveland, Ohio 44135-3191

8. PERFORMING ORGANIZATION REPORT NUMBER

E-11808-1

9. SPONSORING/MONITORING AGENCY NAME(S) AND ADDRESS(ES)

National Aeronautics and Space Administration
Washington, DC 20546-0001

10. SPONSORING/MONITORING AGENCY REPORT NUMBER

NASA TM—2000-209381-REV1

11. SUPPLEMENTARY NOTES

James E. Simpson and Suresh V. Garimella, School of Mechanical Engineering, Purdue University, West Lafayette, Indiana 47907-1968 (work funded by NASA Cooperative Agreement NCC3-476), and Henry C. de Groh III, NASA Glenn Research Center. Responsible person, Henry C. de Groh III, organization code 6712, (216) 433-5025.

12a. DISTRIBUTION/AVAILABILITY STATEMENT

Unclassified - Unlimited
Subject Categories: 23, 26, 29, and 34 Distribution: Nonstandard

This publication is available from the NASA Center for AeroSpace Information, (301) 621-0390.

12b. DISTRIBUTION CODE

13. ABSTRACT (Maximum 200 words)

An experimental study of the horizontal Bridgman growth of pure succinonitrile (SCN) and of a succinonitrile—1.0 mol.% acetone alloy (SCN-1.0 mol.% ACE) has been performed. Experiments involving both a stationary thermal field (no-growth case) and a translating thermal field (growth case) were conducted. Growth rates of 2 and 40 μm/s were investigated. For the pure SCN experiments, the velocity field in the melt was estimated using video images of seed particles in the melt. Observations of the seed particles indicate that a primary longitudinal convective cell is formed. The maximum velocity of two different particles which traveled along similar paths was the same and equal to 1.49 ± 0.01 mm/s. The general accuracy of velocity measurements is estimated to be ±0.08 mm/s, though the data shows consistency to within ±0.02 mm/s. The shape of the solid/liquid interface was also quantitatively determined. The solid/liquid interface was stable (non-dendritic and non-cellular) but not flat; rather it was significantly distorted by the influence of convection in the melt and, for the growth case, by the moving temperature boundary conditions along the ampoule. It was found that the interface shape and position were highly dependent on the alignment of the ampoule in the apparatus. Consequently, the ampoule was carefully aligned for all experiments. The values for front location agree with those determined in previous experiments. For the alloy experiments, the solid/liquid interface was determined to be unstable at growth rates greater than 2.8 μm/s, but stable for the cases of no-growth and growth at 2 μm/s. When compared to the shape of the pure SCN interface, the alloy interface forms closer to the cold zone, indicating that the melting temperature decreased due to the alloying element. Extensive temperature measurements were performed on the outside of the ampoule containing pure SCN. The resulting thermal profiles are presented in detail in the results section. It is intended that the interface shape, thermal boundary condition and velocity data presented in this paper be used to test numerical simulations.

14. SUBJECT TERMS	15. NUMBER OF PAGES
Solidification; Convection; Solute	73
	16. PRICE CODE: A04

17. SECURITY CLASSIFICATION OF REPORT	18. SECURITY CLASSIFICATION OF THIS PAGE	19. SECURITY CLASSIFICATION OF ABSTRACT	20. LIMITATION OF ABSTRACT
Unclassified	Unclassified	Unclassified	